

UNIVERSIDAD SAN FRANCISCO DE QUITO USFQ

Colegio de Ciencias e Ingenierías

**Comparative FEA Analysis of Composite Materials Virtual
Microstructures
Proyecto de Investigación**

César Ramiro Rodríguez Sáenz

Ingeniería Mecánica

Trabajo de titulación presentado como requisito
para la obtención del título de
Ingeniero Mecánico

Quito, 02 de mayo de 2019

UNIVERSIDAD SAN FRANCISCO DE QUITO USFQ
COLEGIO DE CIENCIAS E INGENIERÍAS

**HOJA DE CALIFICACIÓN
DE TRABAJO DE TITULACIÓN**

Comparative FEA Analysis of Composite Materials Virtual Microstructures

César Ramiro Rodríguez Sáenz

Calificación:

Nombre del profesor, Título académico

Edison Bonifaz, PhD

Firma del profesor

Quito, 02 de mayo de 2019

Derechos de Autor

Por medio del presente documento certifico que he leído todas las Políticas y Manuales de la Universidad San Francisco de Quito USFQ, incluyendo la Política de Propiedad Intelectual USFQ, y estoy de acuerdo con su contenido, por lo que los derechos de propiedad intelectual del presente trabajo quedan sujetos a lo dispuesto en esas Políticas.

Asimismo, autorizo a la USFQ para que realice la digitalización y publicación de este trabajo en el repositorio virtual, de conformidad a lo dispuesto en el Art. 144 de la Ley Orgánica de Educación Superior.

Firma del estudiante: _____

Nombres y apellidos: César Ramiro Rodríguez Sáenz

Código: 00123869

Cédula de Identidad: 1718948779

Lugar y fecha: Quito, 02 de mayo de 2019

RESUMEN

Se desarrolló un modelo de elementos finitos de microestructura de material compuesto virtual en 3D para simular los efectos del tamaño de malla y la entrada de material en el comportamiento mecánico de los materiales compuestos isotrópicos. La teoría de los elementos finitos y los elementos de volumen representativos (RVE) representados estadísticamente se utilizaron como la estrategia principal para el modelado constitutivo. El software de código abierto DREAM3D Versión 6.5.83 junto con el código ABAQUS® se usó para generar, analizar y procesar el tipo de fase de la característica, el tamaño de la característica, la forma y la distribución del modelo de elementos finitos. Se probaron siete RVE de material compuesto de diferente tamaño de malla, entrada de comportamiento de material y resolución para investigar la relación entre tamaño de malla, comportamiento de entrada de material y resolución con el comportamiento constitutivo final del compuesto, así como la relación de propiedades mecánicas en la micro y macro escala. Las muestras virtuales se sometieron a una carga de tensión monotónica continua y condiciones de contorno simétricas. Se observan los efectos del tamaño de malla, la entrada de material y la resolución. Los resultados dictan que los niveles más altos de esfuerzo se encuentran en los finales bruscos en las características y la proximidad a las regiones fronterizas. Además, a medida que aumenta el tamaño de la malla, la respuesta del material implicará una mayor tensión. Se recomienda un estudio adicional sobre la influencia del tamaño de la malla en las proximidades de $40 \mu\text{m}^3$, ya que los resultados obtenidos se asemejan mucho al comportamiento mecánico del resultado esperado.

Palabras clave: representative volume element, materiales compuestos, FEM, isotrópico, análisis comparativo

ABSTRACT

A 3D virtual composite material microstructure finite element model was developed to simulate the effects of mesh size and material input on the mechanical behavior of isotropic composite materials. Finite element theory and statistically generated Representative Volume Elements (RVEs) were used as the main strategy for the constitutive modeling. The open-source software DREAM3D Version 6.5.83 coupled with the ABAQUS[®] code were used to generate, analyze and process the feature phase type, feature size, shape, and distribution of the finite element model. Seven composite material RVEs of different mesh size, material behavior, and resolution were tested to investigate the relationship between mesh size, material behavior, and resolution (magnification of features) with the final constitutive behavior of the composite, and the relationship of mechanical properties in the micro and macro scale. The virtual samples were subjected to a continuous monotonic strain load and symmetric boundary conditions. The effects of the mesh size, material behavior, and resolution were observed. Results demonstrate sharp endings on the features and proximity to the boundary regions account for higher levels of stress. Moreover, as mesh size increases, material response involves higher stress. A further study on mesh size influence in the 40 μm^3 vicinity is recommended, as the results obtained closely resemble the mechanical behavior of the expected output.

Keywords: representative volume element, composite materials, FEM, isotropic, comparative analysis

TABLE OF CONTENTS

INTRODUCTION.....	10
METHODOLOGY	14
RESULTS.....	35
CONCLUSIONS.....	44
REFERENCES.....	45
ATTACHMENT A: Input Data for the *PLASTIC Option	47
ATTACHMENT B: Test Sample Visuals	48
ATTACHMENT C: Sample Stress Distributions.....	49

LIST OF TABLES

Table 1. Material parameters	18
Table 2. Data input for the *ELASTIC option	27
Table 3. Sections associated with their material properties	28

LIST OF FIGURES

Figure 1. Modulus of Elasticity v. density (Ashby, 2011).....	10
Figure 2. Material processing as it affects the structure and properties of the material (Jackson, 2013).....	11
Figure 3. Hierarchy of microstructural features (Jackson, 2013)	11
Figure 4. Specific strength and modulus of composites and metals (Barbero, 2011)	12
Figure 5. Outline of the capabilities of the DREAM.3D code (Groeber, n.d.).....	14
Figure 6. RVE composite material (Groeber, n.d.).....	14
Figure 7. Stress-Strain response of various fibers (Herakovich, 1997)	15
Figure 8. Stress-strain responses of epoxy (Cabral & Boster, 2010).....	16
Figure 9. Data extracted shown in the curve (Rohatgi, 2010)	17
Figure 10. Data acquired by the extraction software (Rohatgi, 2010).....	17
Figure 11. Stress-strain response for epoxy	18
Figure 12. Stress-strain response S-glass fibers.....	19
Figure 13. Stress and strain behavior for S-glass and epoxy	19
Figure 14. Phase properties of the fibers	20
Figure 15. Phase Properties of the matrix	20
Figure 16. ESD Probability Density Function	21
Figure 17. Initialize Synthetic Volume Filter	22
Figure 18. Establish shape types filter	22
Figure 19. Establish matrix shape filter	23
Figure 20. Find Feature Neighbors filter	23
Figure 21. Insert Precipitate Phase filter.....	24
Figure 22. Write DREAM.3D Data File filter	24
Figure 23. Abaqus Hexahedron Exporter filter.....	25
Figure 24. DREAM.3D Pipeline.....	25
Figure 25. Files generated by the pipeline	26
Figure 26. XDMF file in PARAVIEW	26
Figure 27. Imported INP file.....	27
Figure 28. Creation of <i>dummy</i> node.....	28
Figure 29. Ending of the general INP file.....	29
Figure 30. An RVE constrained with boundary conditions and a continuous monotonic strain load applied along the y axis (Baus, 2016)	30
Figure 31. FEM assembly (Yang, n.d.).....	31
Figure 32. FEM main framework (Yang, n.d.)	32
Figure 33. Sample management.....	33
Figure 34. TEST 3 model.....	33
Figure 35. Composite partitioned model for TEST3: a) fibers and b) matrix	34
Figure 36. Stress-strain curves from all samples	35
Figure 37. Stress and strain behavior of TEST3 and TEST4.....	36
Figure 38. TEST3 stress distribution; as a composite deformation scale: 10 (top), fiber (bottom left), and matrix (bottom right).....	37
Figure 39. TEST4 stress distribution; as a composite scale deformation: 5 (top), fiber (bottom left), and matrix (bottom right)	38
Figure 40. TEST3 maximum stress	39
Figure 41. Maximum stress TEST4	39
Figure 42. Stress-time and strain-time response for TEST3.....	40

Figure 43. Stress-time and strain-time responses of TEST4.....	41
Figure 44. Size effect of the elastic input samples against the experimental result.....	42
Figure 45. Epoxy curve used as input (orange), and epoxy curve tested experimentally (blue)	43

INTRODUCTION

Composite materials, such as carbon fiber composites, have become important structural materials for critical applications since they can be customized to exhibit properties such as a very high Modulus of Elasticity while maintaining a low density (Tane, Okuda, & Tanaka, 2019). As seen in the Ashby chart below, the composite materials group maintains a low strength to weight ratio critical for applications such as aircraft design, where one of the main objectives is to minimize weight.

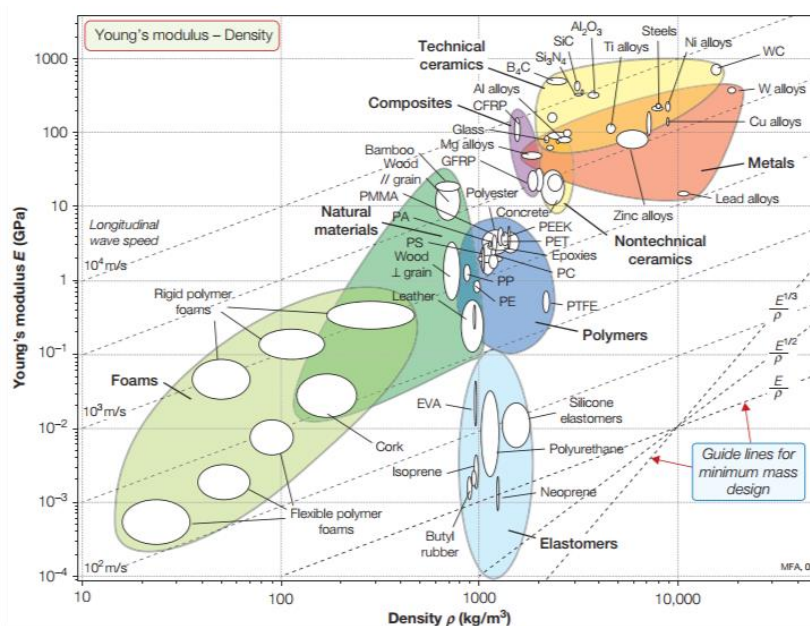


Figure 1. Modulus of Elasticity v. density (Ashby, 2011)

Computational modeling of composite materials, therefore becomes an important design study in critical parts and components where objectives are such as weight reduction, corrosion resistance, wear resistance, etc. Especially fiber-reinforced composite, since materials are a lot stronger in fiber form than in bulk form (Barbero, 2011).

More and more, software allows to develop stronger and more exact computational models to better extract information and try to anticipate and design for more reliable parts. Understanding and considering anisotropy in materials is very critical in engineering processes,

since in every step of manufacturing, the material structure and properties are changed, this happening at the micro scale, as it can be seen in the figure below.

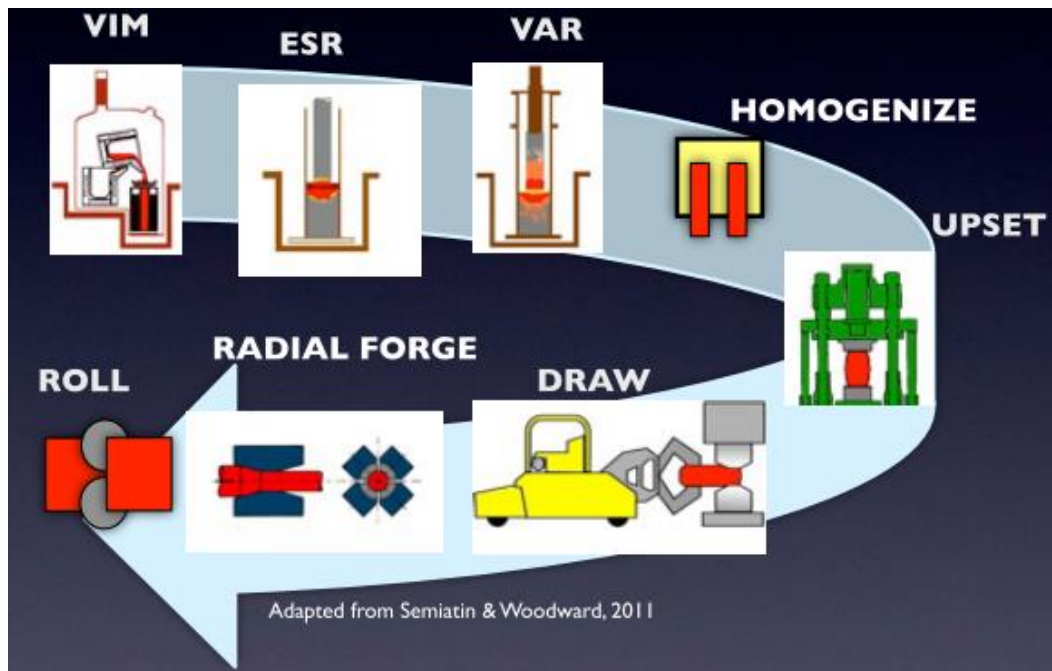


Figure 2. Material processing as it affects the structure and properties of the material (Jackson, 2013)

Moreover, as stated, each microstructure feature modified in the steps of manufacturing, affects the overall properties and performance of the new material. The following graph illustrates the issue of hierarchy of microstructural features.

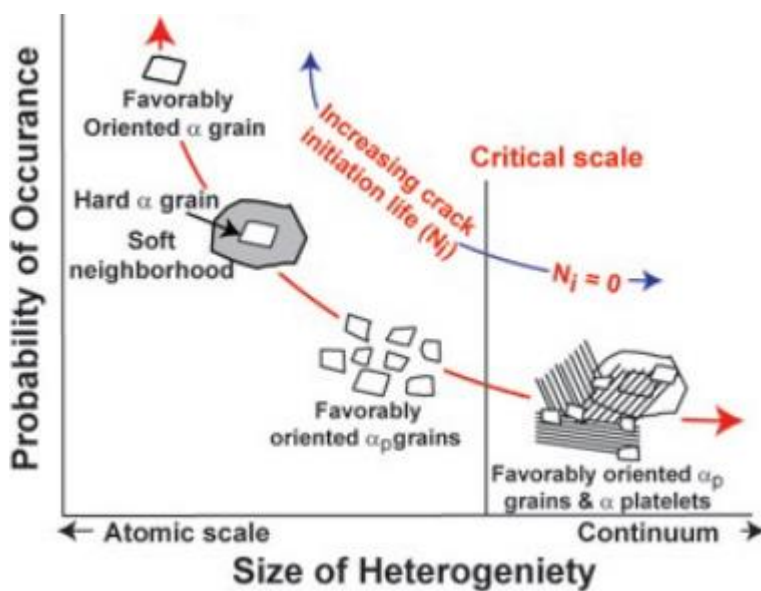


Figure 3. Hierarchy of microstructural features (Jackson, 2013)

This, paired with the modern advancements of manufacturing techniques and exploration on new materials and their properties will result in a trend of more and more applications turning to composite materials as their choice of material (Barbero, 2011).

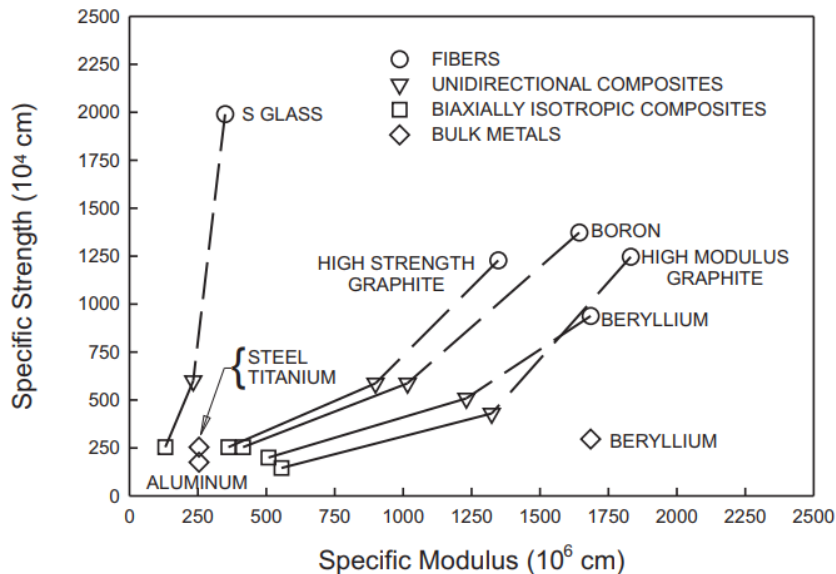


Figure 4. Specific strength and modulus of composites and metals (Barbero, 2011)

The objective of this research project is to develop a mechanical analysis of composite materials at the microstructure level by combining and implementing the DREAM.3D and ABAQUS codes on statistically generated samples of fiber-reinforced composite materials. While the specific objectives rely on determining an accurate size of the sample microstructure, determining an appropriate load case to analyze the sample, defining a sample material combination of matrix and fibers, and determining an appropriate laminate stacking sequence for the composite.

At the micro level, an RVE (representative volume element) encompasses a good estimation of how the material properties are going to behave at the macro level. The definition according to continuum mechanics of an RVE is a volume that represents a composite material statistically; meaning, a volume small enough to represent macroscopic properties, but large enough that boundary conditions remain independent. This means that homogenized properties of a composite can be computed from simulating a single representation of a heterogeneous

medium, such as an RVE of a composite material (Song, Krishnaswamy, & Pucha, 2016). Previously, when implementing a micromechanics-based model, RVE models usually take into consideration a single fiber surrounded by a matrix. Other parameters to be taken into consideration is the fact that the volume fraction of this matrix would have to be the same as the volume fraction of the fibers in the laminate (Naghdasab, Farrokhabadi, & Madadi, 2018).

The use of empirical, and semiempirical models for microstructure modelling has some benefits and drawbacks. Therefore, a solid, well-built composite material model at the micro scale can be obtained by complementing both numerical and analytical models (Naghdasab et al., 2018). Many numerical studies have been developed in order to understand the micromechanics behind a composite laminate since the current knowledge available about failure mechanisms for composites is not enough to develop a sense of physical criteria for some types of failure (Távora, Mantič, Graciani, & París, 2016). This results in the key issue of a representative volume element in the case of composite materials, which results in the linking between the characteristics found at the micro scale to the arbitrary variation of properties at the macro scale (Savvas, Stefanou, & Papadrakakis, 2016).

This research aims to develop a 3D virtual microstructure statistically generated to which one can analyze the mechanical properties of a composite material such as yield stress, maximum strain, etc. Open source software such as ABAQUS and DREAM.3D will be used to simulate and generate these microstructures.

Consequently, it is expected that the mechanical simulation results vary within an acceptable margin with each other, depending on the variation of parameters explained further in the following chapters. Moreover, the simulation is expected to output insightful results since the scope of the research is developed at the micro level.

METHODOLOGY

A representative volume element, or RVE, will be statistically generated using the open source software DREAM.3D, which stands for Digital Representation Environment for Analysis of Microstructure in 3D. This software can generate microstructures depending on a variety of parameters which can be binary files, a set of images, or statistically representative inputs depending on the expected outcome. After the microstructure is generated, it can be exported to different analysis software.

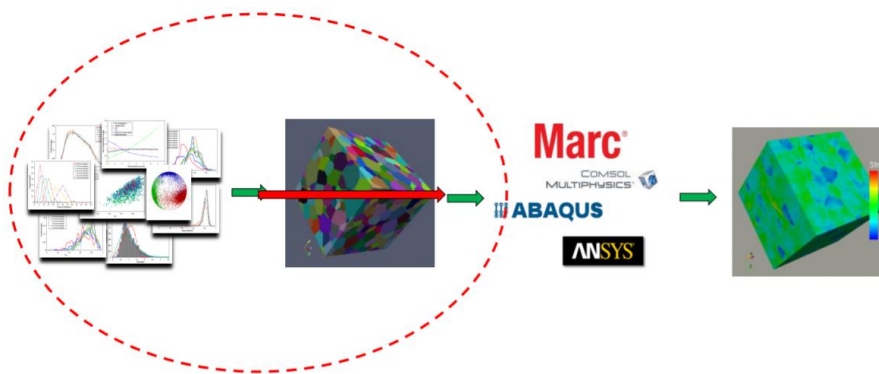


Figure 5. Outline of the capabilities of the DREAM.3D code (Groeber, n.d.)

The software's primary focus is to develop microstructures based on statistical descriptions. With this data, a statistically generated composite microstructure will be created, such as the one below.

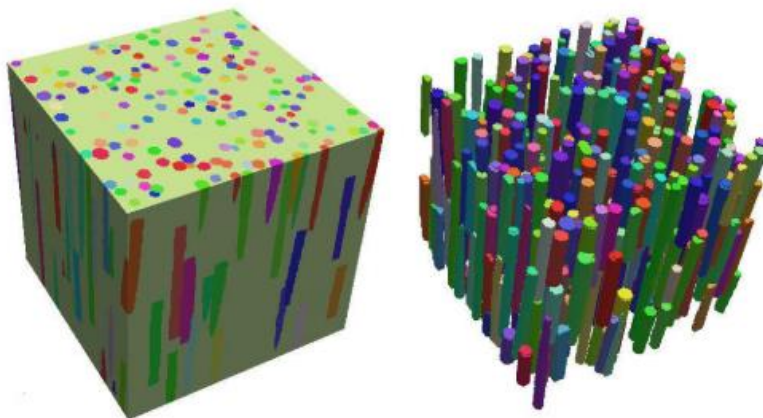


Figure 6. RVE composite material (Groeber, n.d.)

For the different sets of RVE generated in this research, epoxy and fiberglass composites will be created, specifically, an S-glass/epoxy composite made up of an epoxy matrix an S-glass type glass fiber (S for strength). This combination of materials was considered since it provides the higher strength glass type fibers critical for structural applications (Barbero, 2011). It is worth mentioning that the behavior of both materials is elastic up to the breaking point, and that both materials exhibit isotropic behavior. The material properties that will serve as input to the FEA analysis were taken from the following figures.

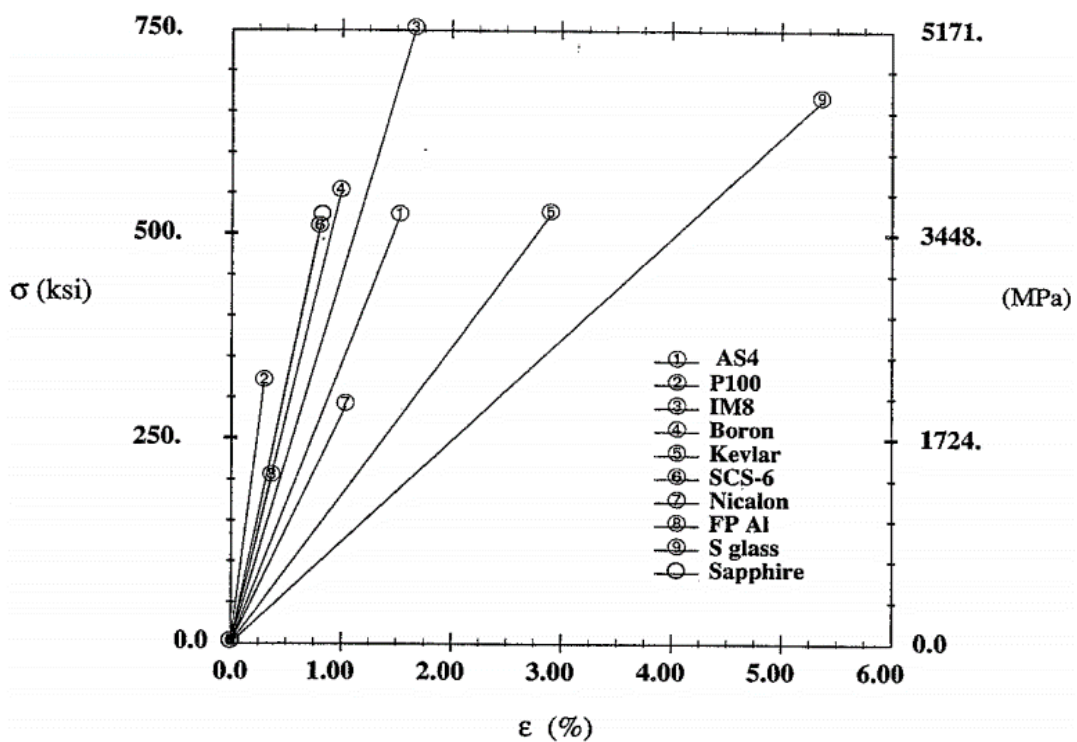


Figure 7. Stress-Strain response of various fibers (Herakovich, 1997)

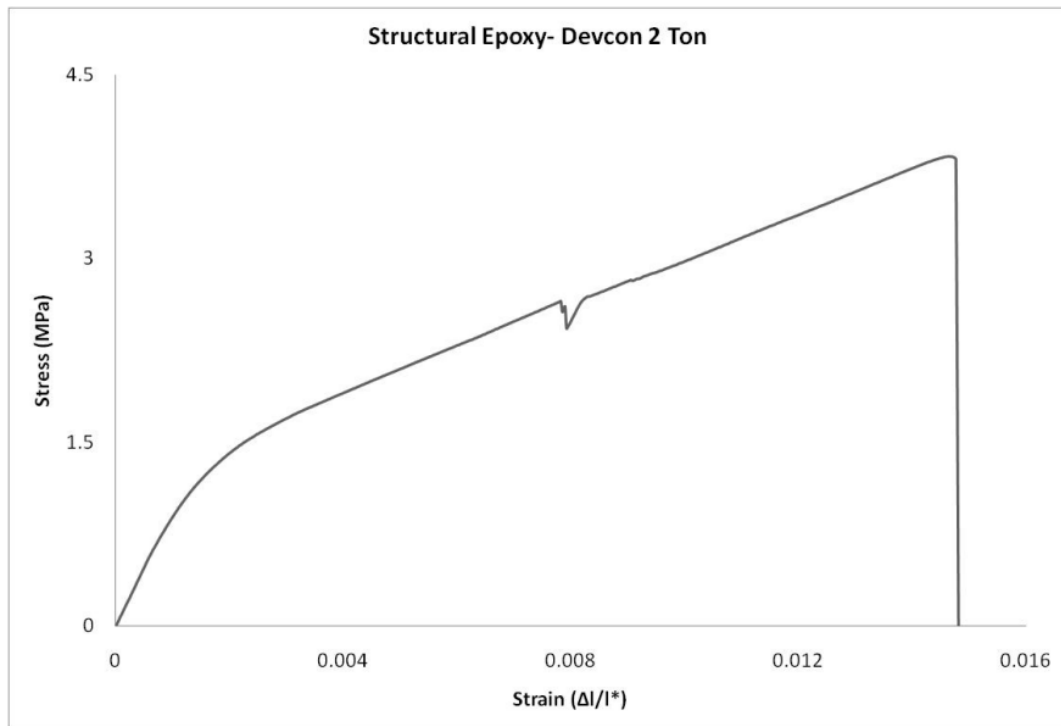


Figure 8. Stress-strain responses of epoxy (Cabral & Boster, 2010)

As it can be appreciated from the figures above, the behavior of both sets of curves is elastic up to the maximum stress point (Gurusideswar, Srinivasan, Velmurugan, & Gupta, 2017). Predictably, the strength behavior of both sets of materials is drastically different, with epoxy reaching around 4 MPa as the ultimate stress and S-glass reaching about 4500 MPa.

Moreover, the data input to the Abaqus FEA code needs an equal set of data for stress and strain for each material. A processing image analysis software was used to extract an equal set of data points (40) from both curves. The process starts by uploading an image and aligning the axes. This process consists on setting 4 points on each of the axis and matching them with the value present on the image. After this process is carried out, a coloring algorithm to highlight the area being analyzed is carried out. This ensures that less mistakes are carried out during the automatic extraction algorithm that will be run. The thickness of the coloring pen can be altered so that more precision can be obtained when coloring narrow parts of the curve where it meets other data or the actual axes. Furthermore, the color of the curve that will be analyzed is chosen among the different colors highlighted in the isolated region.

Moreover, the automatic extraction data is carried out by the *Average Window algorithm* which allows an input for a Δx and Δy value in pixels that will serve as the spacing between each data point. In both data extractions carried out, a value of $\Delta x = \Delta y = 10 \text{ pixels}$ was chosen by default. The extracted data can be seen in the following figure.

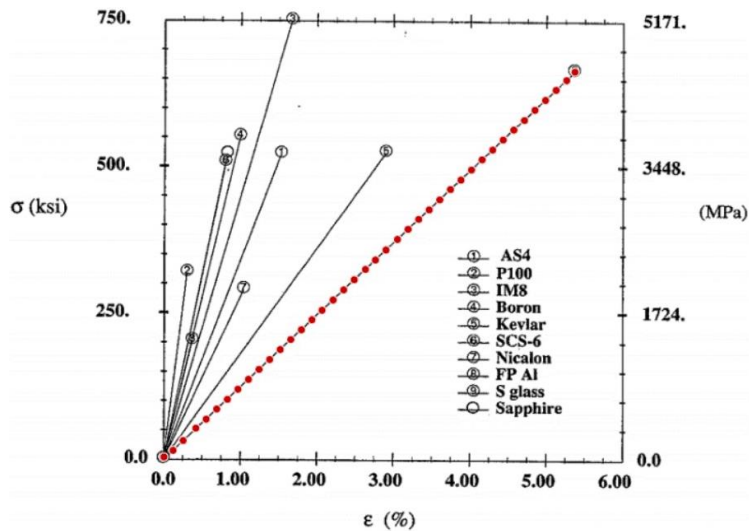


Figure 9. Data extracted shown in the curve (Rohatgi, 2010)

Finally, the data extracted can be sorted, formatted, and copied to be further analyzed or used as input depending on its purpose for extraction as it can be seen on the figure below.

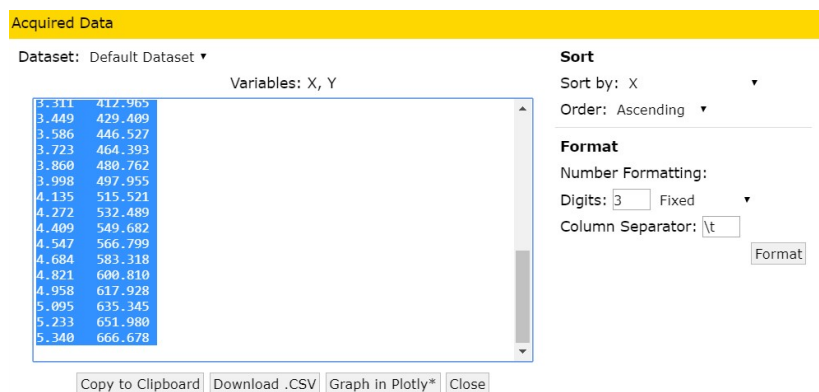


Figure 10. Data acquired by the extraction software (Rohatgi, 2010)

This process was carried out for both figures previously shown corresponding to the stress and strain responses of the S-glass type glass fibers and epoxy matrix. Both curves can be seen plotted individually and on the same figure, for perspective, on the following figures.

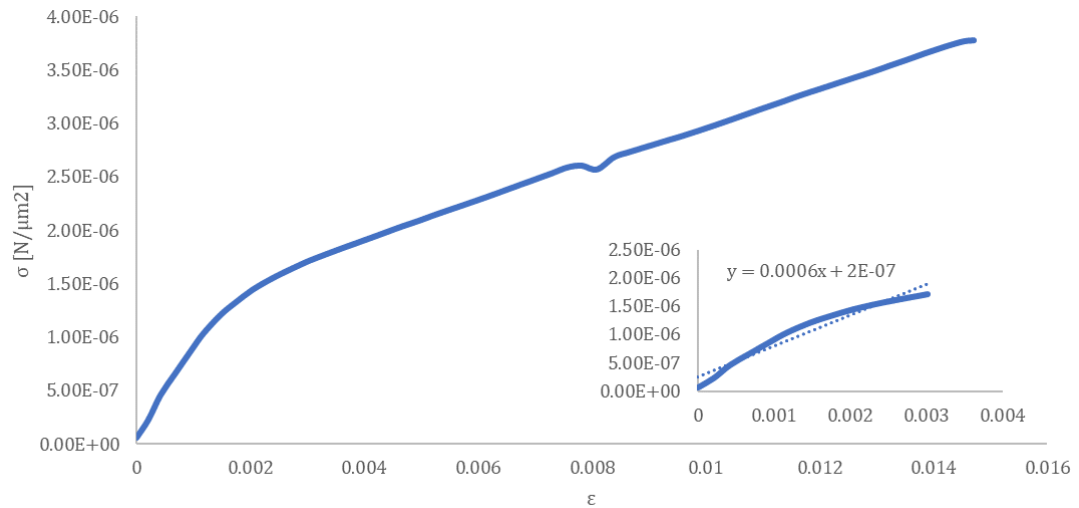


Figure 11. Stress-strain response for epoxy

A linear regression was calculated in order to obtain the Modulus of Elasticity of the epoxy matrix ($E_m = 0.000577467 \frac{N}{\mu m^2} = 577 \text{ MPa}$) which is another input to the Abaqus FEA code, as well as Poisson's ratio of 0.38, commonly attributed to a 9310 Structural Epoxy (Barbero, 2011) as can be seen in the following table.

Table 1. Material parameters

Parameter	Matrix	Fiber	S-glass/Epoxy	Reference
Tensile Modulus, E	-	85 GPa	-	(Barbero, 2011)
Poisson's ratio, ν	0.38	0.22	-	(Barbero, 2011)
Fiber volume fraction, V_f	-	-	0.6	(Barbero, 2011)

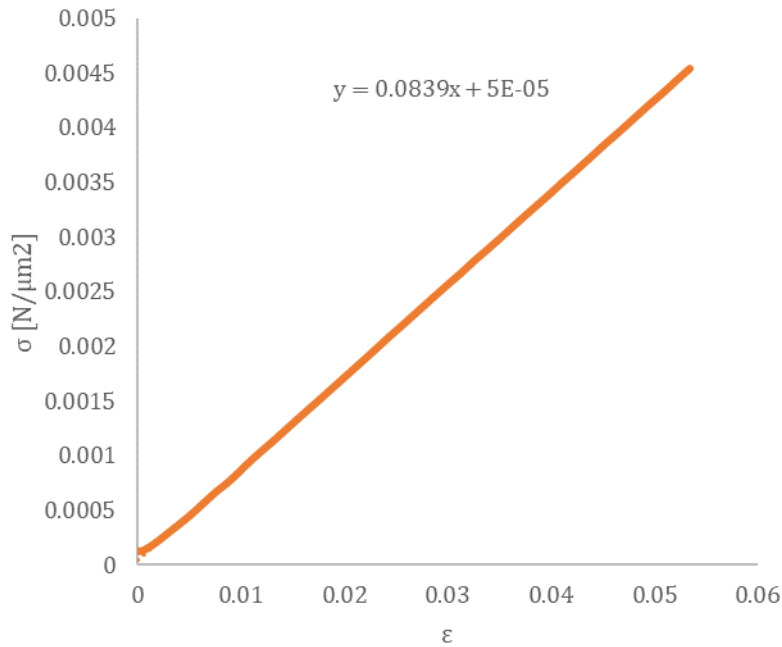


Figure 12. Stress-strain response S-glass fibers

The same process was carried out with the fibers, in which a Modulus of Elasticity of $E_f = 0.0839 \frac{\text{N}}{\mu\text{m}^2} \approx 85 \text{ GPa}$ was found from the linear regression.

Together, the stress and strain responses for the constitutive materials are represented on the figure below. Unsurprisingly, the linear-elastic tendencies and the drastic difference between the ultimate stresses is what gives the composite its performance and material design capability.

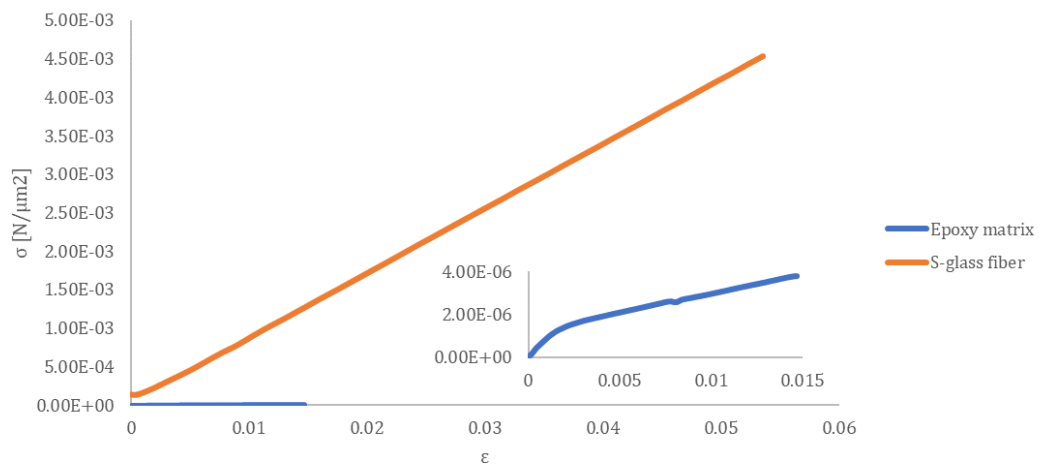


Figure 13. Stress and strain behavior for S-glass and epoxy

After establishing the properties of the material, the different RVEs will be created using the open-source software DREAM.3D. This software uses a set of filters, that together form a pipeline, which will be executed in order to develop the final meshed product.

First, the stats generator filter will give the different phases its properties. Input parameters include the equivalent sphere diameter (ESD), phase fraction, phase type, etc. The following figures show the Phase Properties of both the matrix and the fibers.

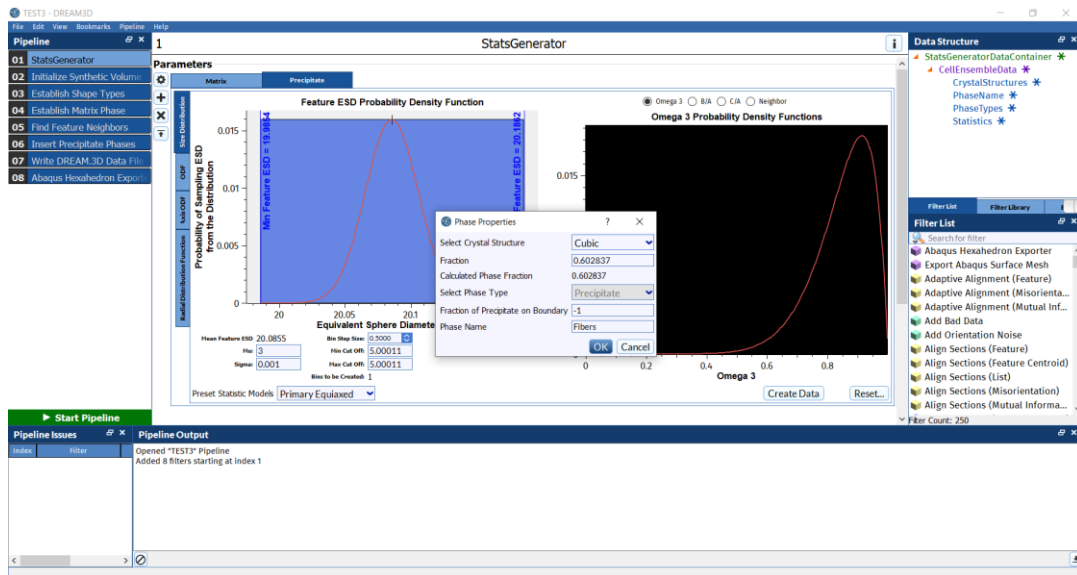


Figure 14. Phase properties of the fibers

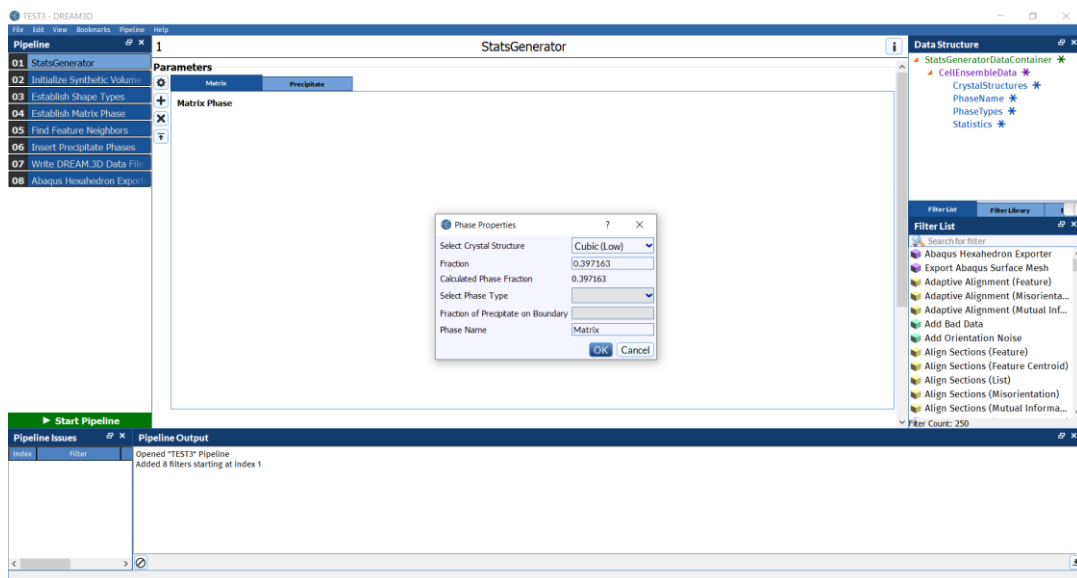


Figure 15. Phase Properties of the matrix

For this research, a fiber volume fraction of $V_f = 0.6$, as stated previously.

Similarly, the estimated sphere diameter (ESD), corresponding to the fiber diameter will be set to around $20 \mu\text{m}$, an average glass fiber diameter (Cihan, Sobey, & Blake, 2019). This can be set by varying the parameters that make up the ESD Feature Probability Density Function μ and σ .

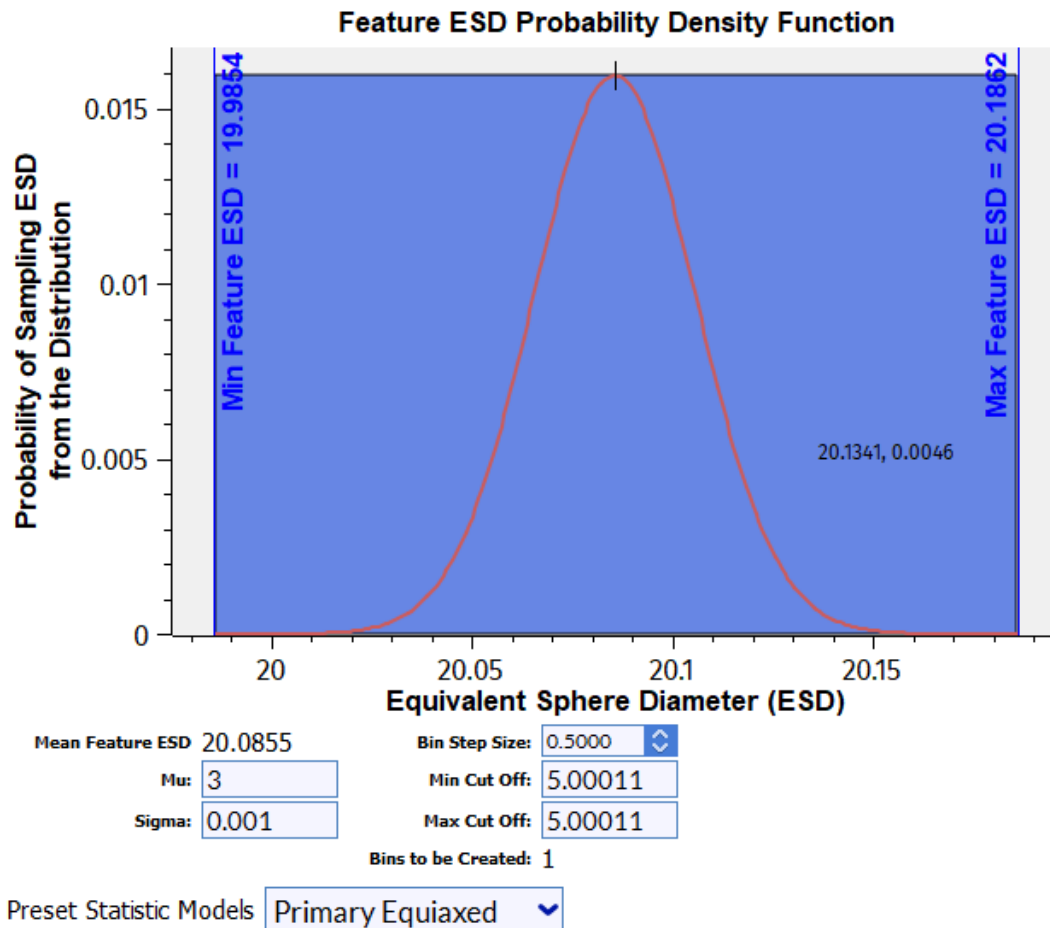


Figure 16. ESD Probability Density Function

The next filter to apply is the Initialize Synthetic Volume which creates an empty volume where you can create/edit dimensions, resolutions, origins as it is illustrated in the figure below.

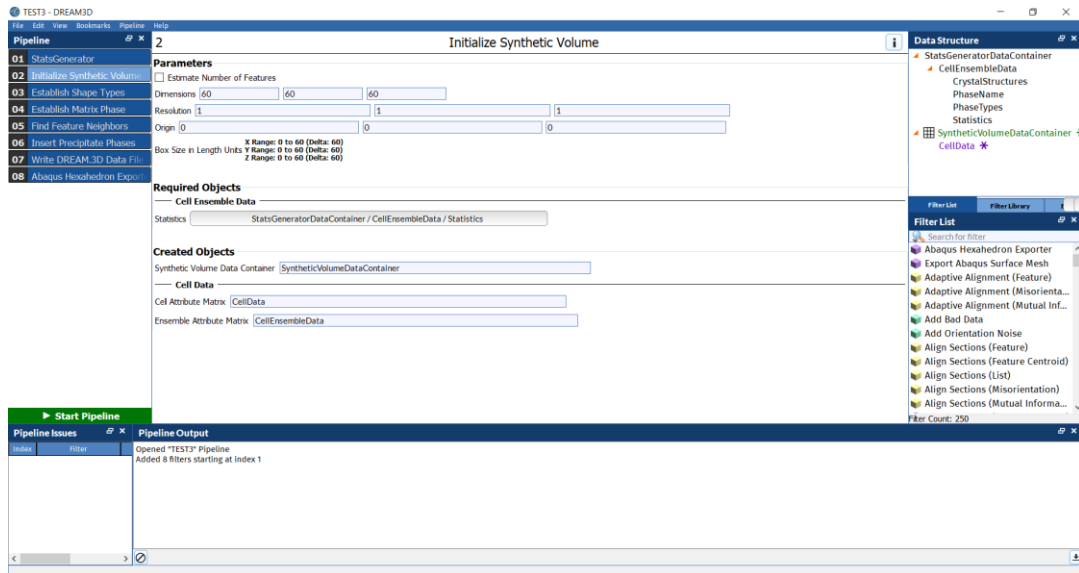


Figure 17. Initialize Synthetic Volume Filter

As seen above, the dimensions for this example are 60x60x60 microns with a resolution of 1 micron per cell and a conventional coordinate system of (0, 0, 0).

Up next, the Establish shape types filter is applied which establishes the morphology of the phases of the microstructure being created. In this case, both the matrix and the fibers have been chosen to have an ellipsoid-like morphology.

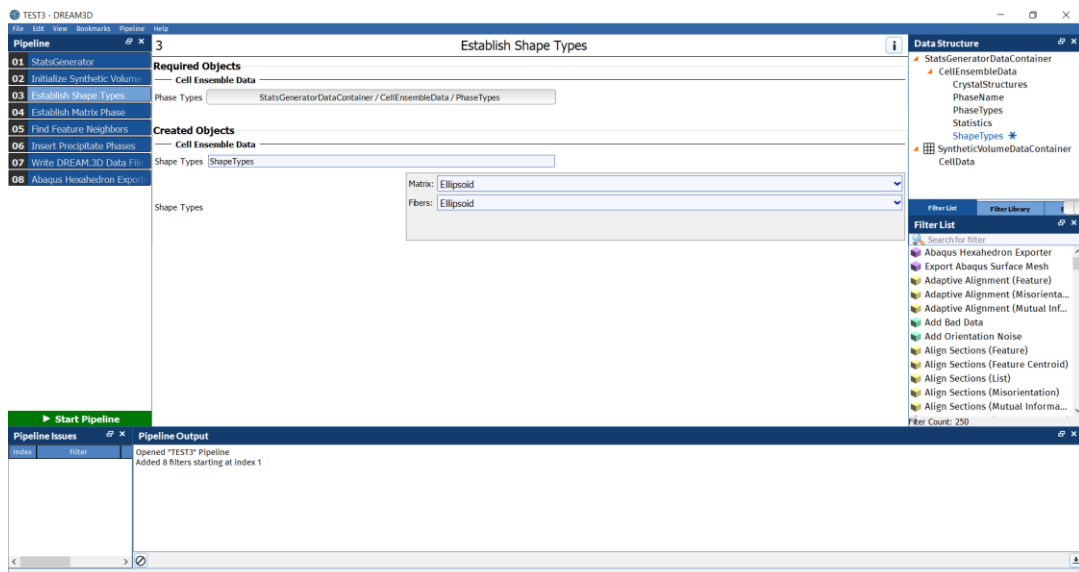


Figure 18. Establish shape types filter

Additionally, the Establish Matrix Phase filter is selected in which the shape of the matrix is created for the virtual microstructure.

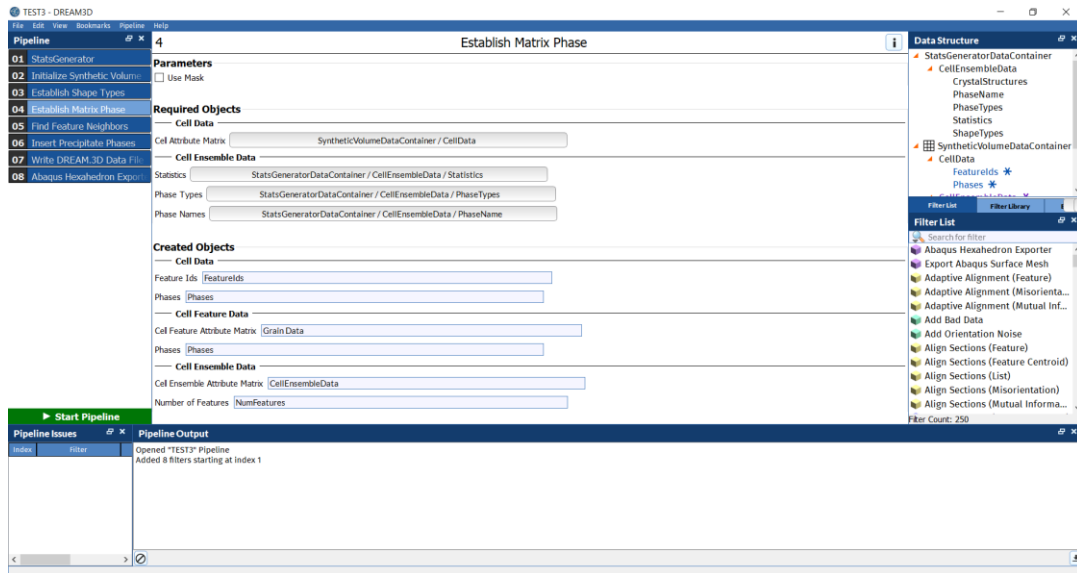


Figure 19. Establish matrix shape filter

Moreover, the next filter to apply is the Find Feature Neighbors filter which determines the number of features that are in contact with the main feature. This filter can be seen in the figure below.

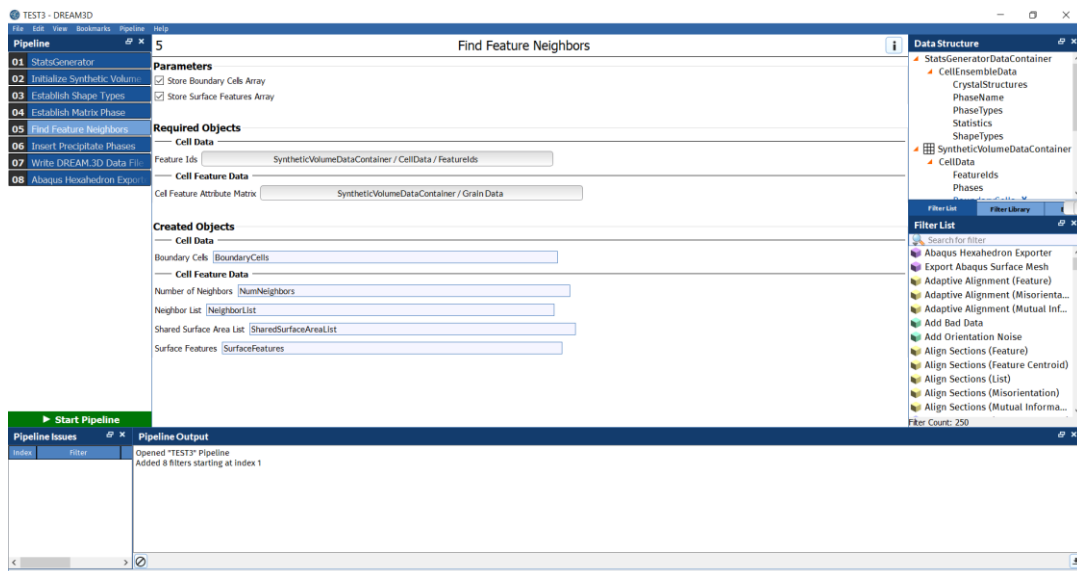


Figure 20. Find Feature Neighbors filter

Subsequently, the insert precipitate phases filter inserts the precipitate phase created previously in the volume generated. This filter is visible in the figure below.

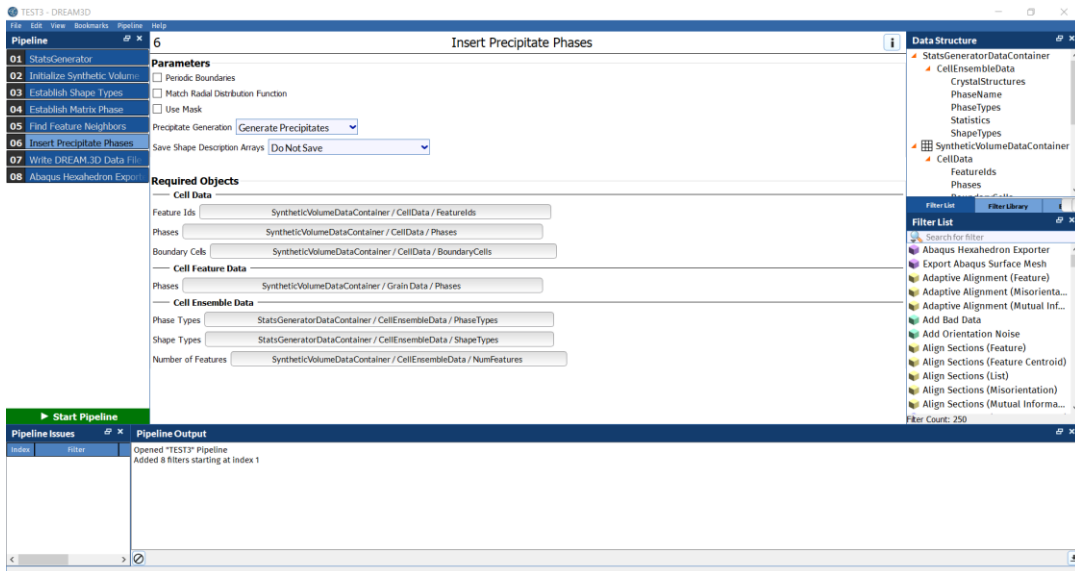


Figure 21. Insert Precipitate Phase filter

The next filter to be applied is the Write DREAM.3D Data File. This creates a DREAM.3D file and has the option to parallelly create an XDMF file visible in PARAVIEW. The directory of the output file needs to be created.

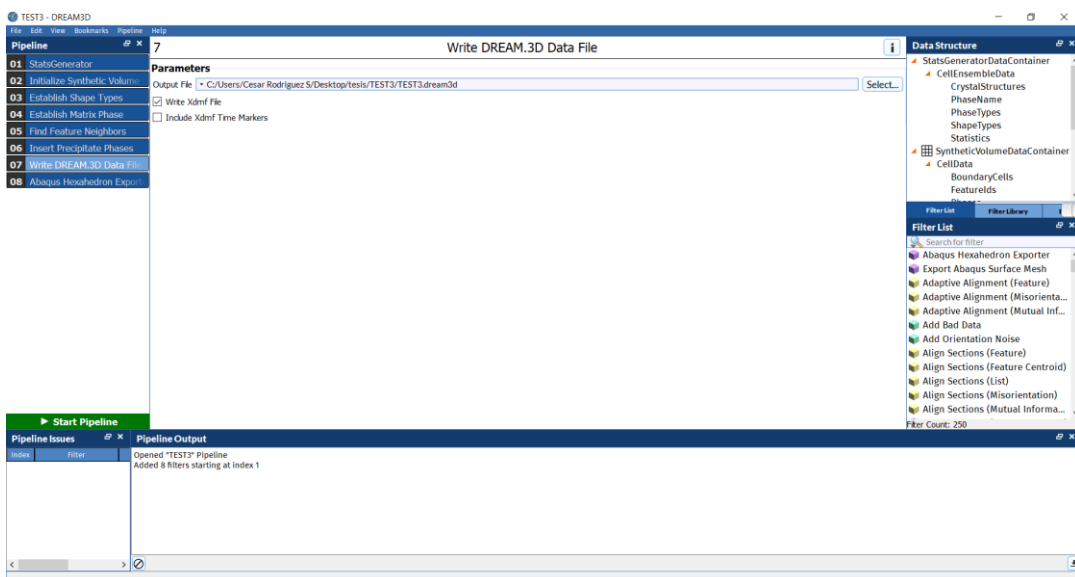


Figure 22. Write DREAM.3D Data File filter

Finally, the last filter corresponds to the Abaqus Hexahedron Exporter which creates a set of 5 .inp files useful to import to the Abaqus FEA code. The output path for these files needs to be specified, as well as the Job Name, and the prefix for the set of .inp files.

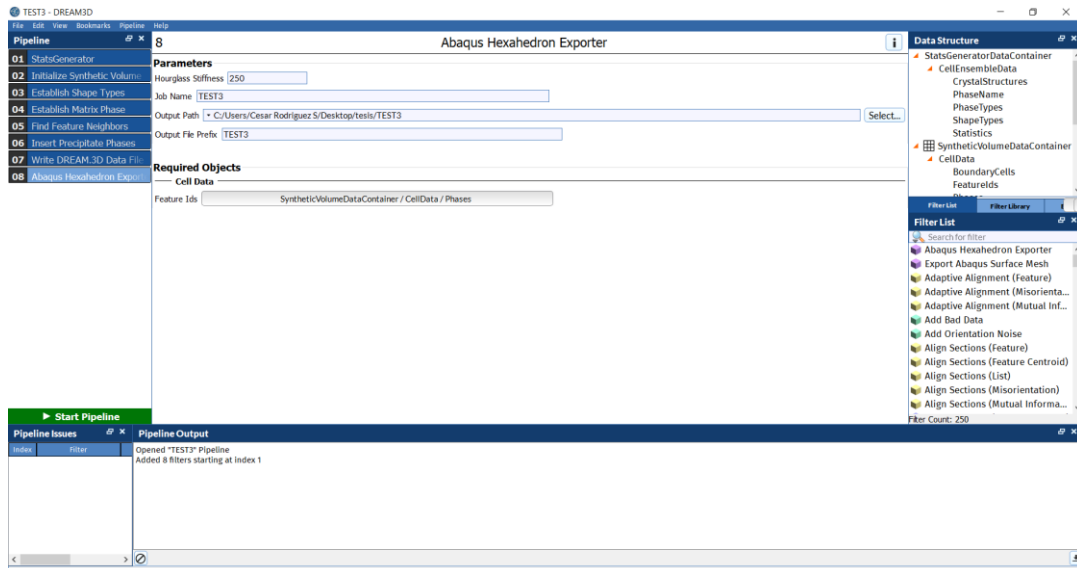


Figure 23. Abaqus Hexahedron Exporter filter

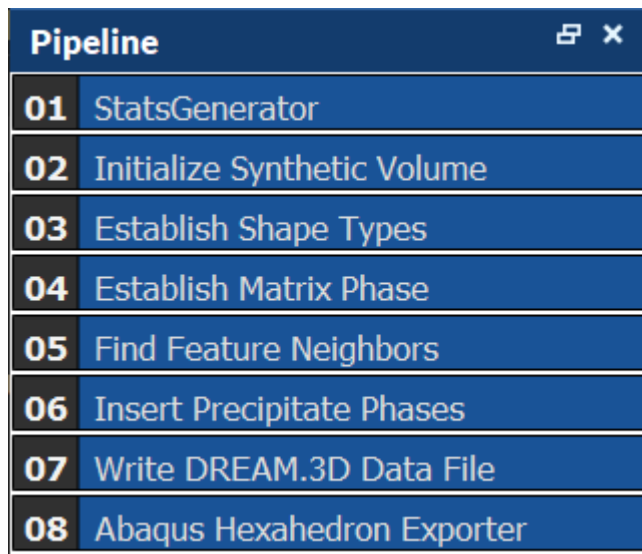


Figure 24. DREAM.3D Pipeline

The set of 8 filters shown in the figure above has created a pipeline which is now ready to be started. As a result, it will generate 8 files in the output directory specified earlier. These files can be seen in the figure below.

	TEST3	DREAM3D File
	TEST3	INP File
	TEST3_elems	INP File
	TEST3_elset	INP File
	TEST3_nodes	INP File
	TEST3_sects	INP File
	TEST3	JSON File
	TEST3	XDMF File

Figure 25. Files generated by the pipeline

From these files, the JSON file can be used to edit and run the pipeline again while four of the five INP files will be called in a single INP file, in this case the TEST3.inp file which will be imported to the ABAQUS FEA code. The XDMF file can be used to quickly check the microstructure generated using PARAVIEW.

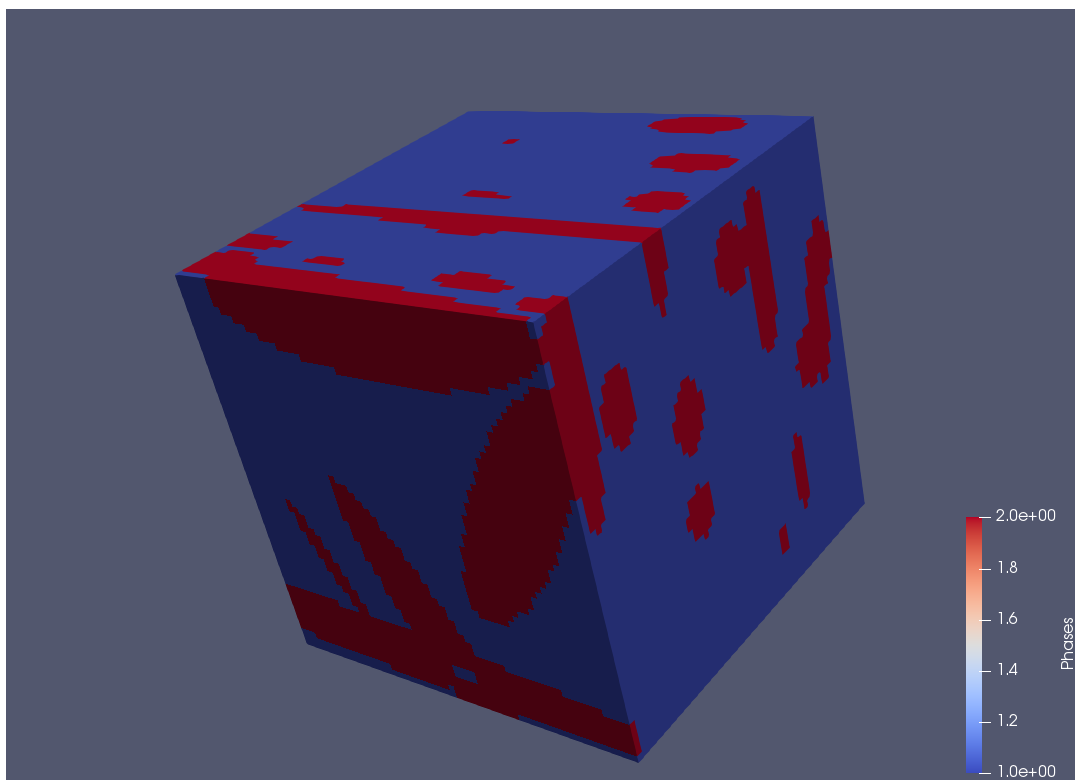


Figure 26. XDMF file in PARAVIEW

Enabling the INP file requires opening the Abaqus CAE software and importing the Model as an INP file extension. The imported INP file will show up with the distinguishable element sets from the matrix and fiber as it can be seen below.

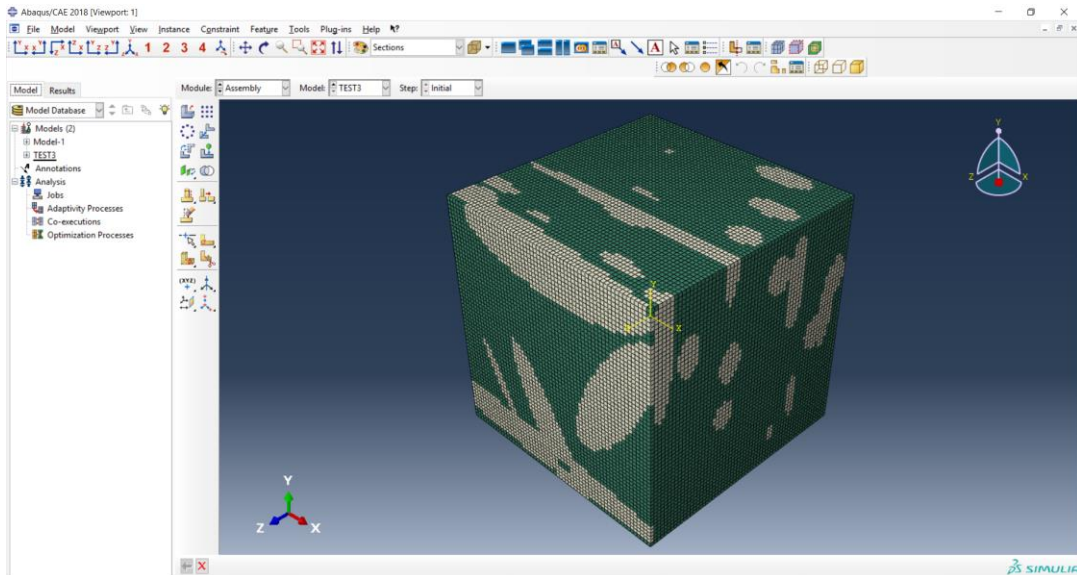


Figure 27. Imported INP file

Following this, symmetry boundary conditions were created with respect to the planes that form the X, Y, and Z axis. Similarly, boundary conditions were applied in the rest of the axes. The *symmetry boundary condition* implies the restriction of rotation in the direction of the other axes the symmetry is not applied to, and the restriction of translation on the axis the symmetry is applied to. Meaning, the XSYMM condition does not allow for rotation around the Y, and Z axes, and does not allow for translation on the X axis.

Material properties were added in the *ELASTIC and *PLASTIC options. In the *ELASTIC option, Young's Modulus and Poisson's Ratio are inputs, while in the *PLASTIC option, Yield Stress and Plastic Strain data sets are inputs. In this example, the following table summarizes the input data for *ELASTIC, while Attachment A summarizes the data used for the *PLASTIC option.

Table 2. Data input for the *ELASTIC option

Material	Young's Modulus [N/ μm^2]	Poisson's Ratio
Epoxy matrix	0.000577	0.38
S-glass fiber	0.085	0.22

Each one of the material properties was associated with its respective section. The following table represents the relationship of each section with its material property.

Table 3. Sections associated with their material properties

Section	Material
Section-1-GRAIN1_SET	Matrix
Section-2-GRAIN2_SET	fiber

A node set was created to associate it with a dummy node in order to obtain reaction forces (RF) in the different time steps by the name DUMMY_NODES. Finally, a job will be created and a general INP file will be generated.

After the general INP file was created, inside the *new* INP file, a node with arbitrary coordinates relating the DUMMY_NODES node set will be created and related to the dummy node, as it is presented below.

```
*NODE,NSET=DUMMY
5000000,25.,25.,55.
*EQUATION
2
DUMMY_NODES,2,1.0,5000000,2,-1.0
*End Assembly
```

Figure 28. Creation of *dummy* node

This dummy node will represent all the nodes on the top surface which will allow to collect all the reaction forces from the top surface where the displacement load was placed. In turn, relating all these reaction forces to one node will output a single total reaction force, RF2, for every time step. It is important that this dummy node is placed inside the assembly, since it needs to be declared as part of the model. In the end of the general INP file, the following lines of code will have to be added in order to control the parameters, state the displacement of the dummy node, and print the displacement (U2) and reaction forces (RF2) data for each time

step. The displacement chosen for this study relies on a 2% elongation based on (Gurusideswar et al., 2017), since the ultimate displacement for epoxy is around 2% of its total length. Given that in this instance, if the matrix fails, the whole composite will fail.

```

*STEP, INC=200, NLGEOM
*STATIC
0.003, 1.0, 1.E-7, 0.3
*CONTROLS, PARAMETERS=FIELD, FIELD=DISPLACEMENT
5.E-1, 1.0, 1.E-1, , , 1.E-4
*BOUNDARY
Set-2, YSYMM
Set-3, XSYMM
Set-4, ZSYMM
DUMMY, 2, 2, 1.2
*NODE PRINT, NSET=DUMMY, FREQ=1
U2, RF2
*OUTPUT, FIELD, FREQ=1, VARIABLE=ALL
*ELEMENT OUTPUT, ELSET=cube
*OUTPUT, HISTORY, FREQ=1, VARIABLE=ALL
*EL FILE
COORD
*ENDSTEP

```

Figure 29. Ending of the general INP file

The results obtained from every time iteration U2, and RF2 correspond to the displacement in the y axis, and the reaction force exerted on the plane defined by the y axis respectively, as it can be shown in the figure below.

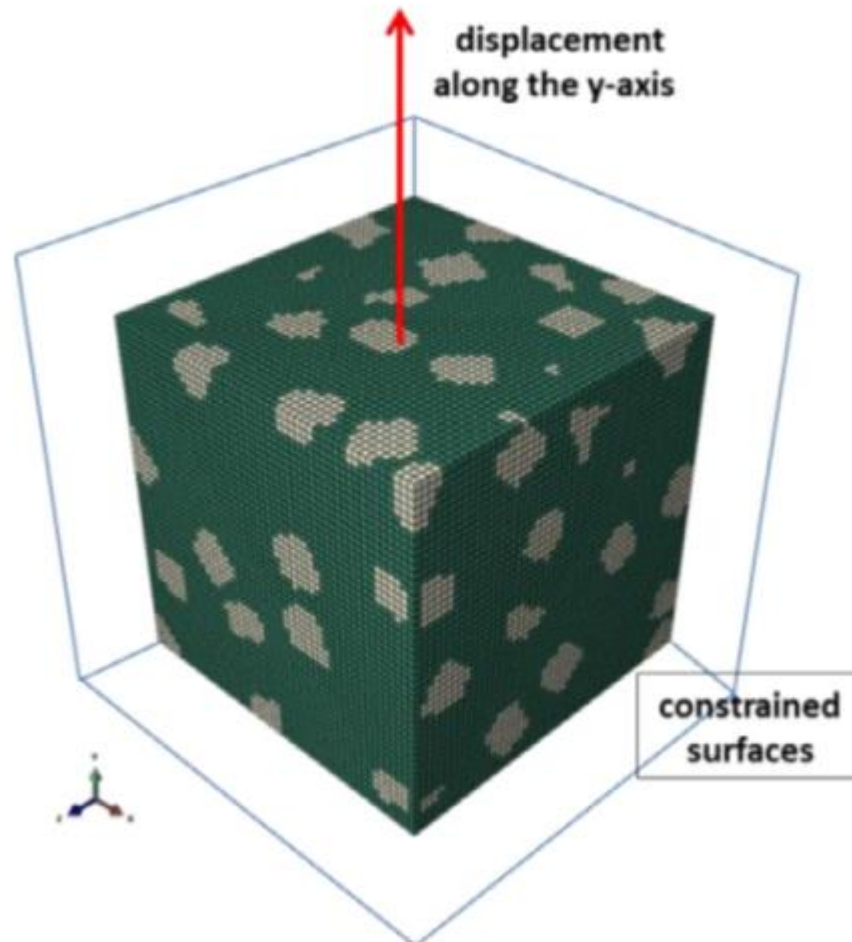


Figure 30. An RVE constrained with boundary conditions and a continuous monotonic strain load applied along the y axis (Baus, 2016)

This pair of results (U2, RF2) will emulate how a tensile stress-strain test occurs when after processing the results for every time iteration, U2 will be divided by the total length of the specimen to find the strain ϵ , and RF2 will be divided by the area perpendicular to that force to find the normal stress σ . This will allow to create a stress-strain curve.

The FEM model embedded in the Abaqus FEA code consists of a numerical method that solves differential equations generated from the complex structure of the part or assembly being analyzed (Yang, n.d.). The process goes by dividing the part/assembly into several non-uniform regions called *finite elements* that will be connected by *nodes*. Each one of these elements has dependent variables at the nodes. An interpolation is defined regarding the values

of the dependent variables at the nodes. This results in a governing algebraic equation for each element.

$$[K]_e\{U\}_e = \{F\}_e \quad (1)$$

Where the subscript e stands for element; the matrix $[K]_e$ is the elementary stiffness matrix, determined by geometry, material, and element properties; the vector $\{U\}_e$ is the elementary displacement vector; and the vector $\{F\}_e$ is the elementary force vector. Moreover, these elementary governing algebraic equations are assembled into a global matrix equation that represents the whole part/assembly to be analyzed.

$$[K]\{U\} = \{F\} \quad (2)$$

The previous process involves stating boundary conditions for which the governing algebraic equations can be solved for the dependent variable at each node (Yang, n.d.). Additionally, stress and strain values can be calculated from the displacement of the nodes solved by the governing algebraic equations.

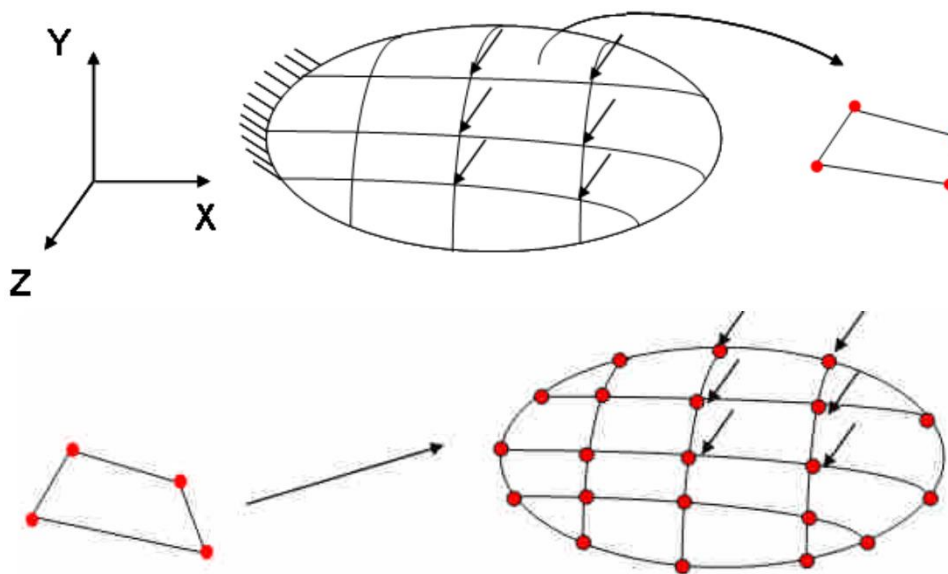


Figure 31. FEM assembly (Yang, n.d.)

The Element Stiffness Matrix is defined as

$$K^e = \int B^T DB dV = B^T DBV \quad (3)$$

Where V is the volume of the element, \mathbf{B} is the strain-nodal displacement matrix, \mathbf{D} is the material property matrix where it is established whether the material is isotropic or anisotropic.

Moreover, the element nodal force vectors are defined as

$$\mathbf{f}_{\varepsilon_0}^e = \int \mathbf{B}^T \mathbf{D} \boldsymbol{\varepsilon}_0 dV = \mathbf{B}^T \mathbf{D} \boldsymbol{\varepsilon}_0 V \quad (4)$$

For the element nodal force vector as a result of self-strain

$$\mathbf{f}_{\sigma_0}^e = \int \mathbf{B}^T \boldsymbol{\sigma}_0 dV = \mathbf{B}^T \boldsymbol{\sigma}_0 V \quad (5)$$

For the element nodal force vector as a result of pre-stresses

$$\mathbf{f}_b^e = \int \mathbf{N}^T \mathbf{b} dV \quad (6)$$

For the element nodal force vector as a result of the body forces

$$\mathbf{f}_s^e = \int \mathbf{N}^T \mathbf{s} dS \quad (7)$$

For the element nodal force vector of the surface tractions

$$\mathbf{f}_{PL}^e = \sum \mathbf{N}^T \mathbf{f}_p \quad (8)$$

For the element nodal force vector as a result of a point load; combined, the composite nodal force vector is represented as

$$\mathbf{f}^e = \mathbf{f}_{\varepsilon_0}^e - \mathbf{f}_{\sigma_0}^e + \mathbf{f}_b^e + \mathbf{f}_s^e + \mathbf{f}_{PL}^e \quad (9)$$

These equations will be solved for every element and assembled in the global matrix equation mentioned previously (Stasa, 2003). Furthermore, the FEM method consists of additional steps that follow a sequence that help provide a better understanding of the model and a better visualization of the results. These steps are illustrated below:

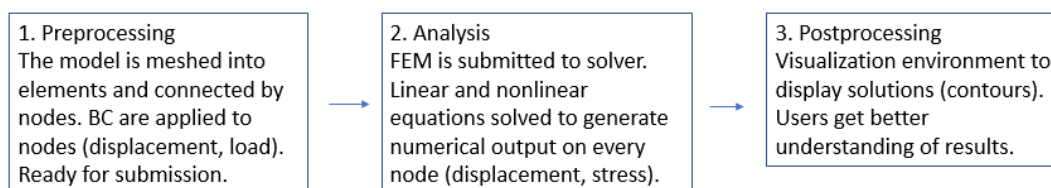


Figure 32. FEM main framework (Yang, n.d.)

Complying with this framework, several comparative tests were developed at a different RVE volume, mechanical behavior response, and resolution. All the tests used the same quasi-isotropic laminate stacking sequence (LSS) of [60/0/-60]. A sample management table is shown below representing these criteria on the tests

No. test	LSS	Volume, μm^3	Elastic/Plastic	Magnification
1	60/0/-60	20	Elastic	1x
2	60/0/-60	40	Elastic	1x
3	60/0/-60	60	Elastic	1x
4	60/0/-60	60	Plastic	1x
9	60/0/-60	60	Elastic	3x
10	60/0/-60	60	Elastic	1.5x
11	60/0/-60	60	Plastic	1.5x

Figure 33. Sample management

These samples were tested using the methodology previously explained. Below, the model for TEST 3 is presented



Figure 34. TEST 3 model

Similarly, the fibers and matrix of TEST 3 can be illustrated in the figure below

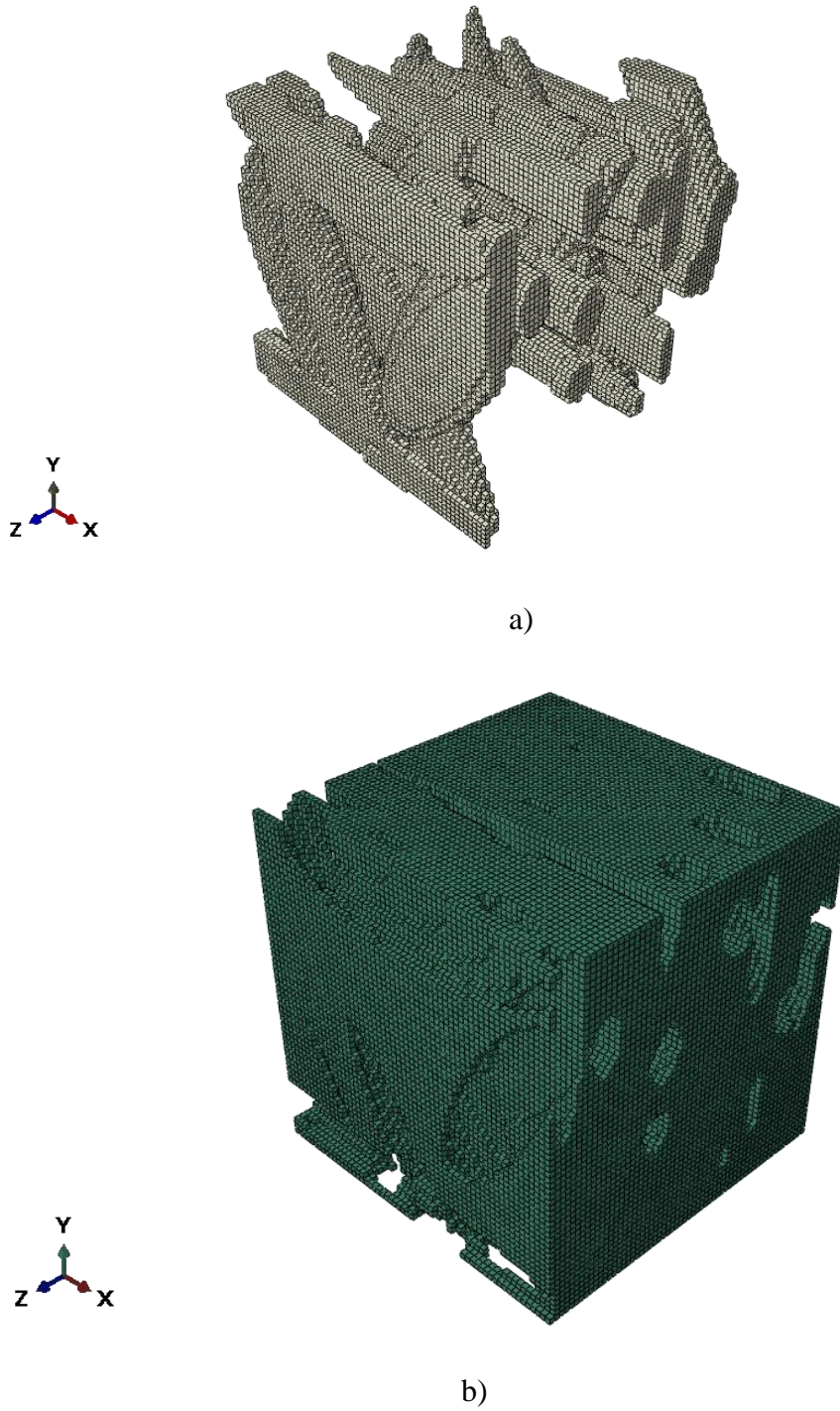


Figure 35. Composite partitioned model for TEST3: a) fibers and b) matrix

RESULTS

Once the simulations ran with the established parameters, the seven samples to be analyzed generated output files that will be explained below. As it can be seen in ATTACHMENT B, the input files vary in mesh size, resolution, and material properties. The volumetric fiber fraction V_f was kept constant, as well as the displacement boundary condition, and the laminate stacking sequence. Stress and strain curves following the methodology explained in the previous section were developed as well as the contour figures generated by the ABAQUS code.

In the figure below, the stress-strain curve of all the samples can be observed, this curve was obtained for a 2% elongation, since as it was explained earlier, the epoxy matrix fails at around that value, and the composite would not perform if the matrix fails, since the behavior of the matrix is non-linear elastic up to the breaking point.

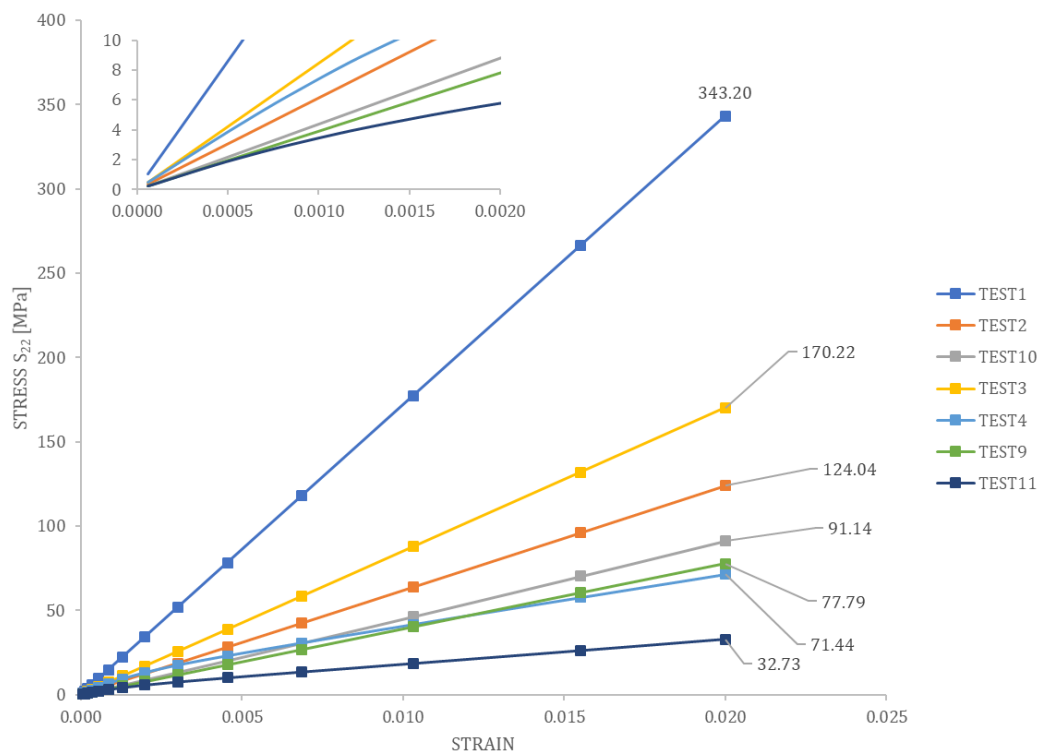


Figure 36. Stress-strain curves from all samples

As it can be seen from the previous figure, TEST1 encompasses the highest level of stress at 343.2 MPa at 2% elongation, as well as the steepest slope, meaning a stiffer material structure. A linear regression was performed to calculate the elastic modulus of this sample at 17.2 GPa .

The behavior exhibited by samples TEST4, TEST9, and TEST10 is similar; the range of stresses is around 70 to 90 MPa, and the curves exhibit a similar slope, meaning a similar material stiffness.

Mesh size is a determining factor to consider since the smaller mesh sizes develop the higher stresses, as it can be observed with tests 1 and 11, where the smallest and largest mesh sizes are considered, at $20 \mu\text{m}^3$ and $60 \mu\text{m}^3$ respectively.

Two samples with the same mesh size and features, TEST3 and TEST4, were simulated with different material inputs. TEST3 has an ELASTIC material input, while TEST4 has an ELASTIC and PLASTIC material input. Their stress and strain curves are illustrated below

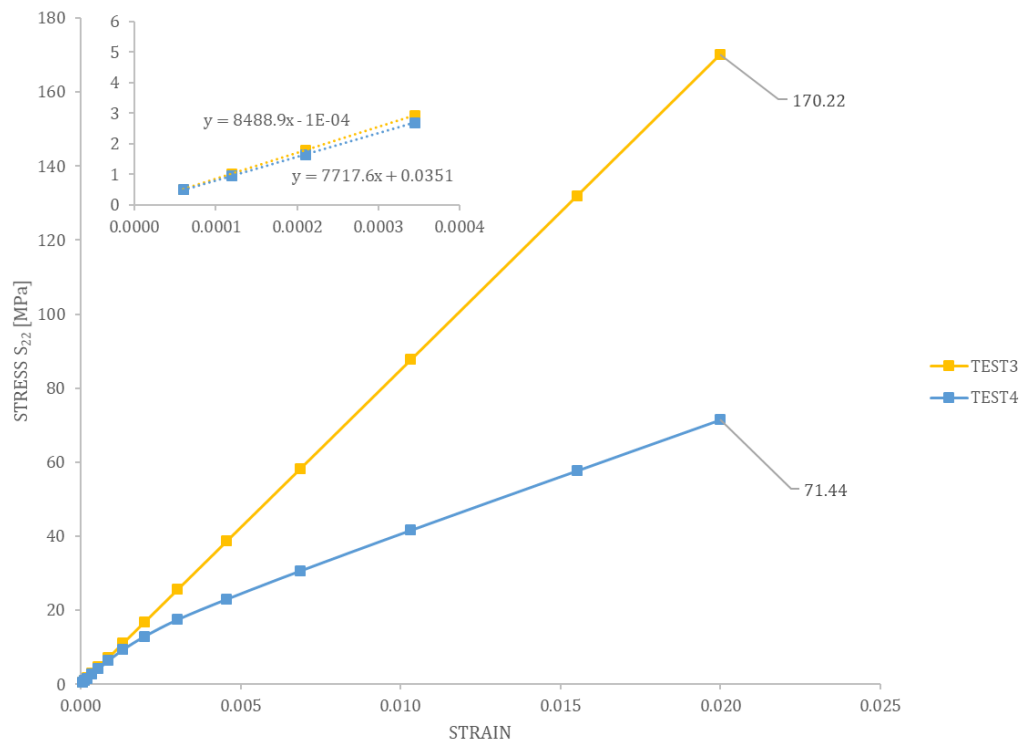


Figure 37. Stress and strain behavior of TEST3 and TEST4

From Figure 36, TEST 3 and TEST4 do not appear to have a similar behavior, the maximum stress point at each one of these samples has a 100 MPa difference. Taking a closer look at Figure 37, the non-linearity of the curve from TEST4 starts from the iteration 4 onwards. Before this divergence, both curves show a similar behavior, with a modulus of elasticity of $E = 8.5 \text{ GPa}$ for TEST3 and $E = 7.7 \text{ GPa}$ for TEST4. The results generated by TEST 3 and TEST4, both with a mesh size of $60 \mu\text{m}^3$, can be seen in the figure below.

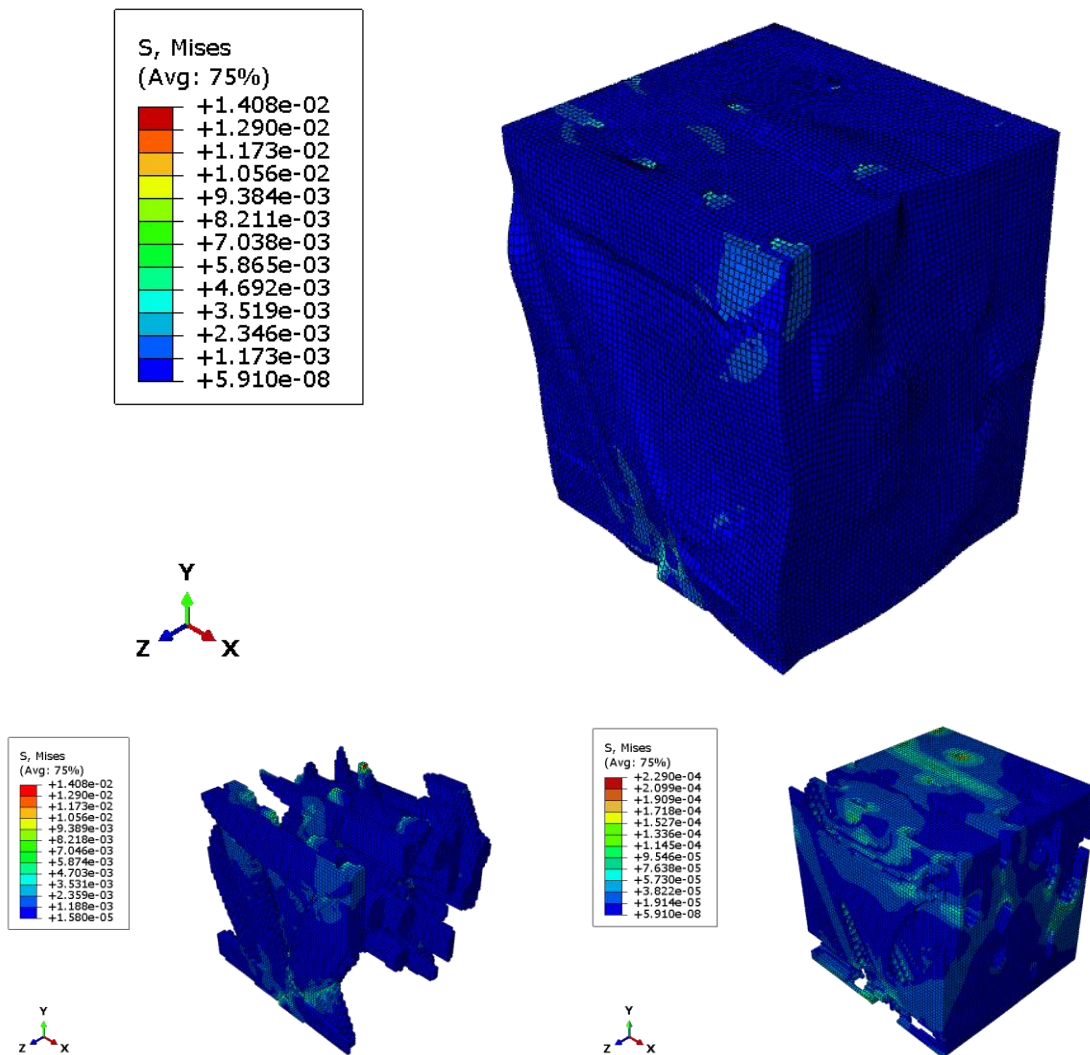


Figure 38. TEST3 stress distribution; as a composite deformation scale: 10 (top), fiber (bottom left), and matrix (bottom right)

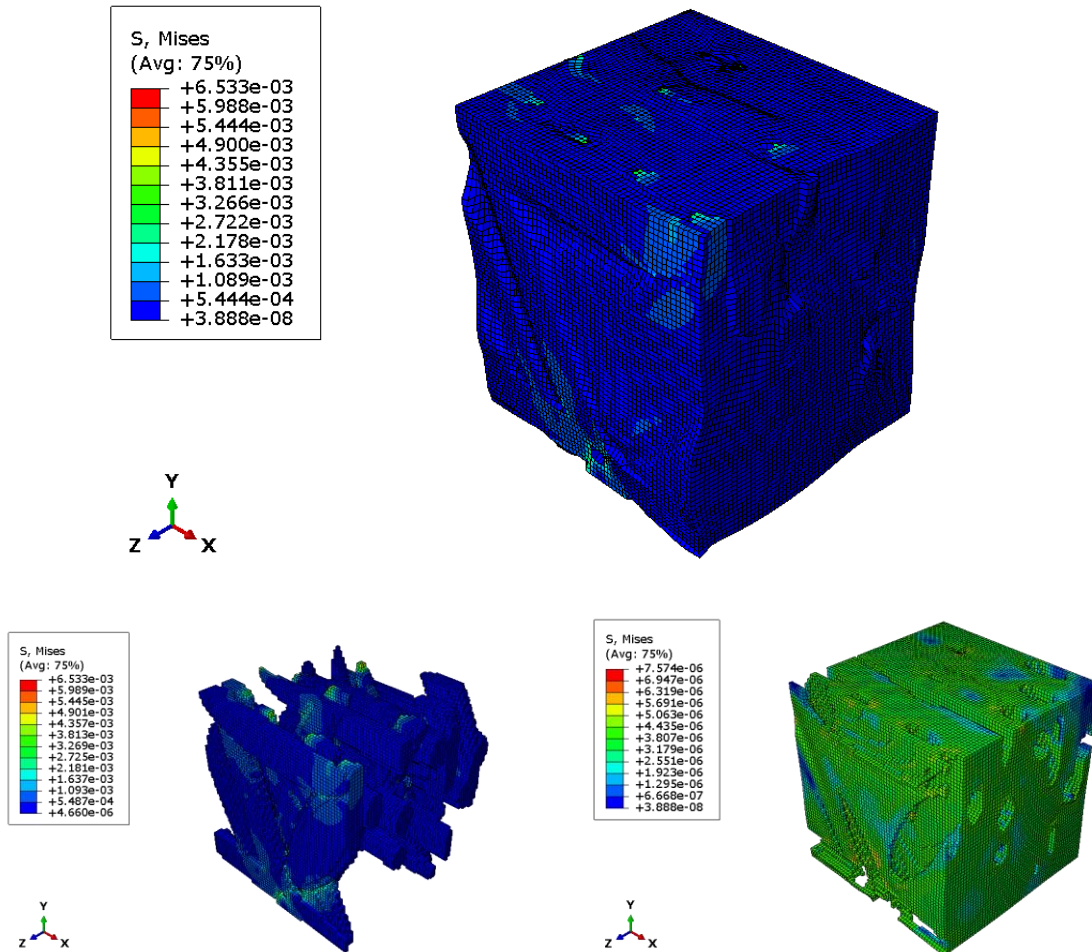


Figure 39. TEST4 stress distribution; as a composite scale deformation: 5 (top), fiber (bottom left), and matrix (bottom right)

From the figures above, the stresses in the model reach levels of 14.08 GPa on TEST3 and 6.5 GPa on TEST4. These regions, where the red contour is located, is where the highest stress concentrator will be located. This means that it will be the location where the failure mode will be initiated. Moreover, as it can be seen in the figures below, this region is in the fibers for both samples.

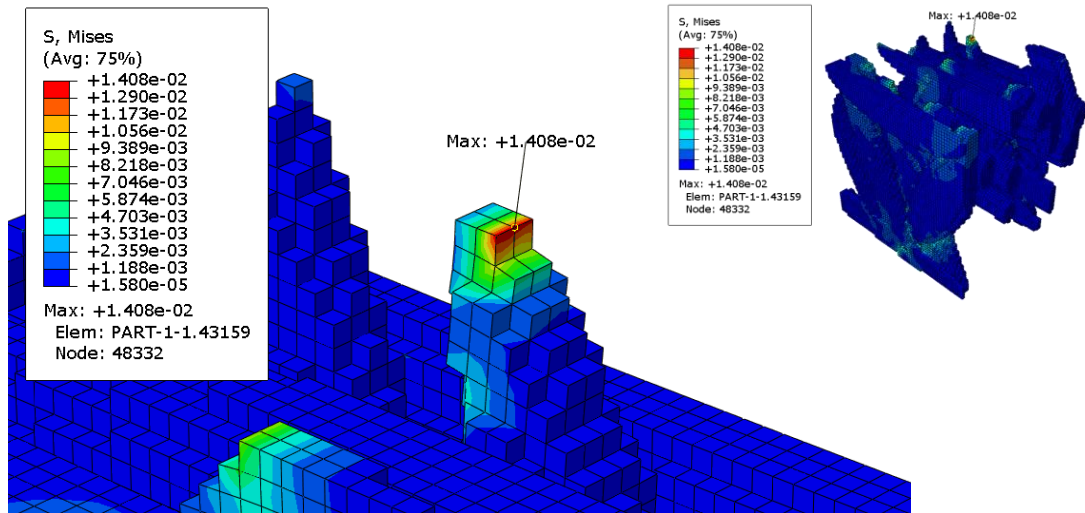


Figure 40. TEST3 maximum stress

As previously stated, the sharp corners and the proximity to the boundary conditions contributes to this location having the highest stress distribution out of the model. The stress distribution for the critical point on TEST4 can be seen below.

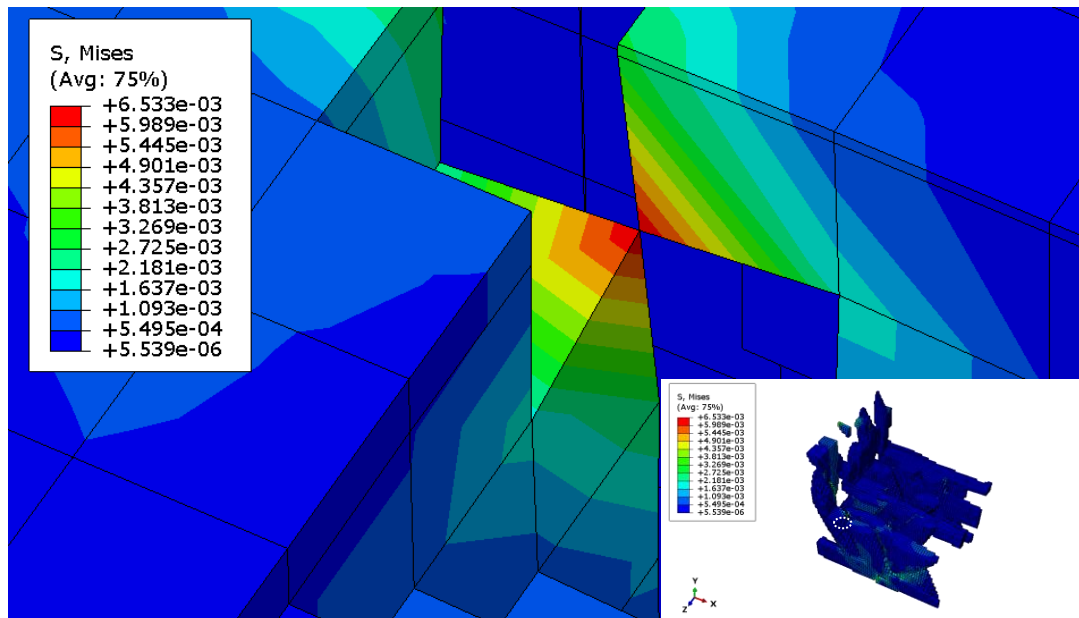


Figure 41. Maximum stress TEST4

The location of this point was found to be inside the model, between two fibers, as seen above, far away from the boundary conditions. This high stress concentrator will most likely originate the mode of failure. In contrast, the rest of the fibers, and the matrix have a uniform distribution of stress, where the fibers hold higher values.

A better overview of how the stress changes throughout the different time steps can be seen in the figures below, where the stress-time and strain-time responses of four elements from the corners of the top surfaces are shown.

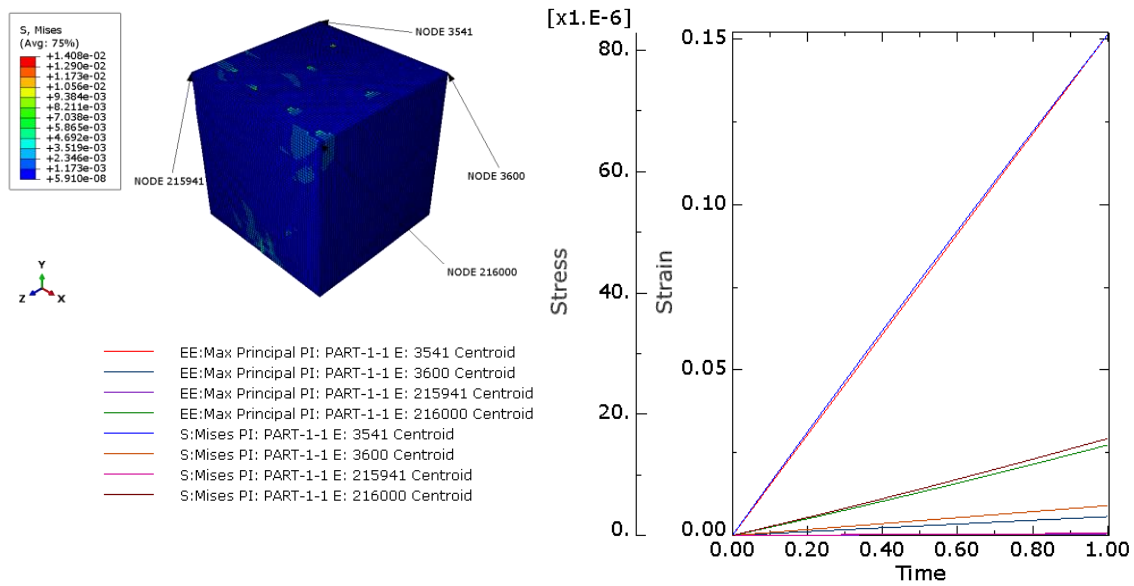


Figure 42. Stress-time and strain-time response for TEST3

The response seen above is linear, as expected. Moreover, NODE 3541, located at the back of the figure above, reaches a higher level of stress than the other nodes in the figure at around 80 MPa , while the other nodes register values close to 15 MPa and 5 MPa . Similarly, NODE 3541 registers the highest strain out of the four at $\epsilon = 0.15$. The location of this NODE is the closest to the maximum achieved stress, as seen on Figure 40.

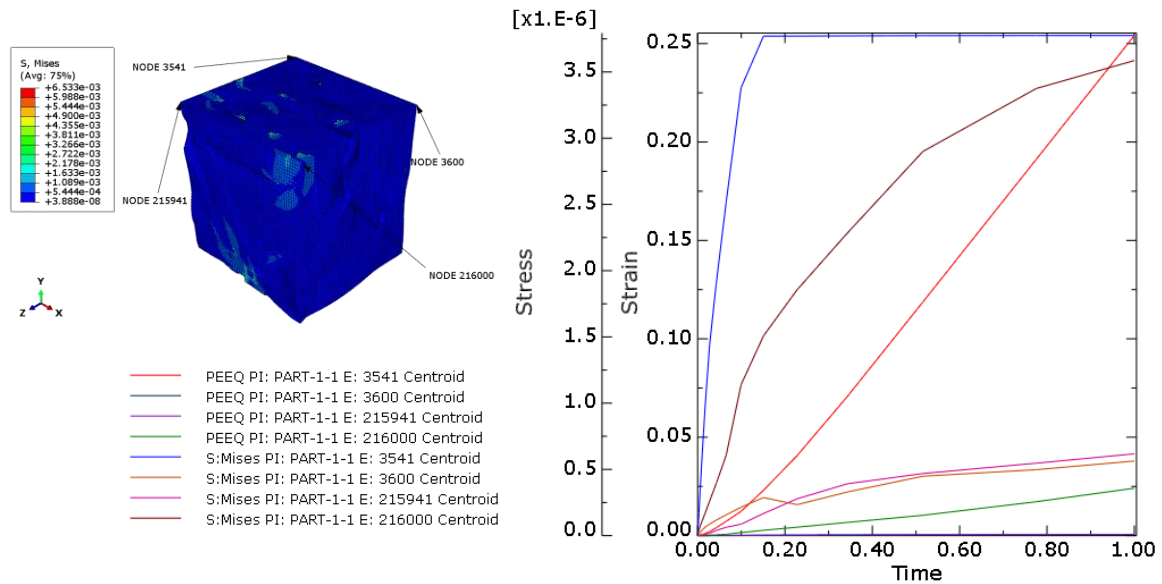


Figure 43. Stress-time and strain-time responses of TEST4

As illustrated in the figure above, the curve behaves as non-linear. The stress achieved on NODE 3541 is the highest, at around 3.75 MPa , while the lowest are shown on NODES 3600 and 215941. Moreover, these nodes achieve almost no plastic strain; which is also observed on Figure 39 by the uniform contour surrounding this region. As previously stated, the results obtained for TEST4 have lower values for stresses, than the values for TEST3. The only difference between these samples was that TEST3 had as an input, an elastic behavior; while TEST4 had a plastic behavior. The results obtained for TEST4 are restricted by the stress-strain curve for both constituting materials.

On the figure below, the influence of the mesh size is illustrated on the stress-strain curves for the samples with an elastic input. Samples TEST1, TEST2, and TEST3 have a mesh size of $20 \mu\text{m}^3$, $40 \mu\text{m}^3$, and $60 \mu\text{m}^3$ respectively; while samples TEST9 and TEST10, both have a mesh size of $60 \mu\text{m}^3$, but a resolution of $3x$ and $1.5x$, respectively. Meaning that the features, at a higher resolution, increase in size the amount of the resolution, while keeping the mesh size.

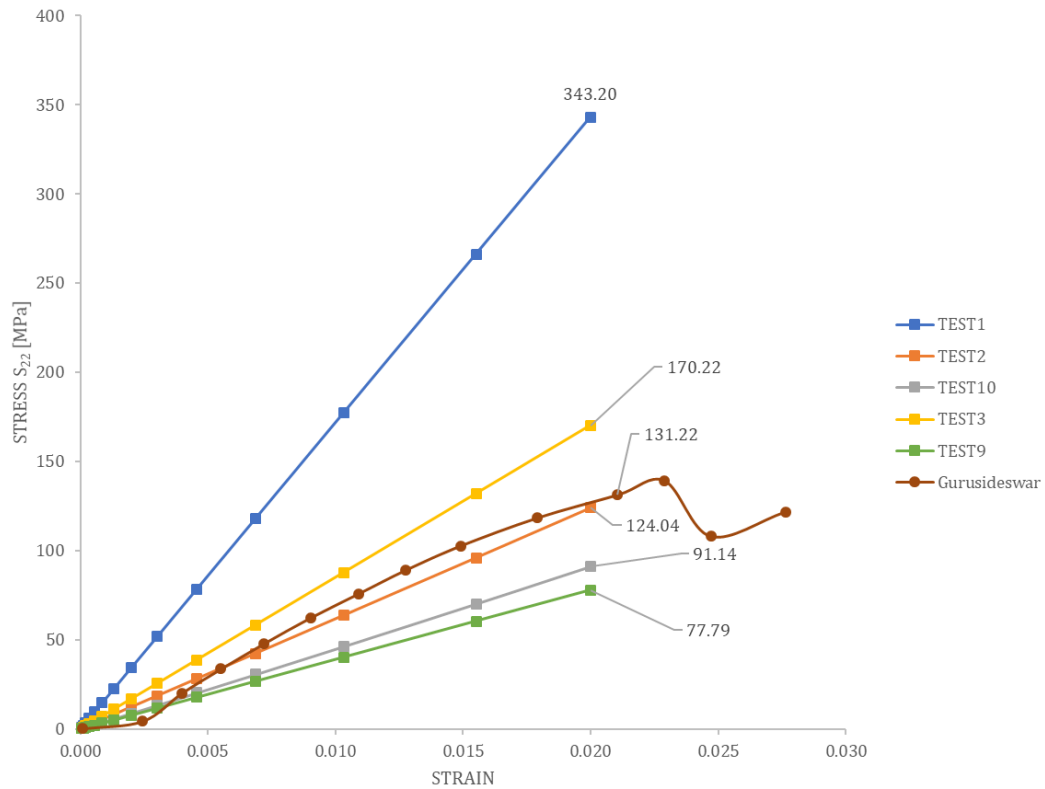


Figure 44. Size effect of the elastic input samples against the experimental result

From the figure above, the closest resemblance to the experimental result (Gurusideswar et al., 2017) relies on TEST2, which shows a comparable level of stress at around the same strain; 124.04 MPa for TEST2, and 131.22 MPa for the experimental result.

It is worth mentioning that the input data used corresponds to a different type of epoxy than the one used to experimentally test the composite above. Below, the curve used as input (Cabral & Boster, 2010) and the epoxy curve from the composite tested experimentally (Gurusideswar et al., 2017) are compared.

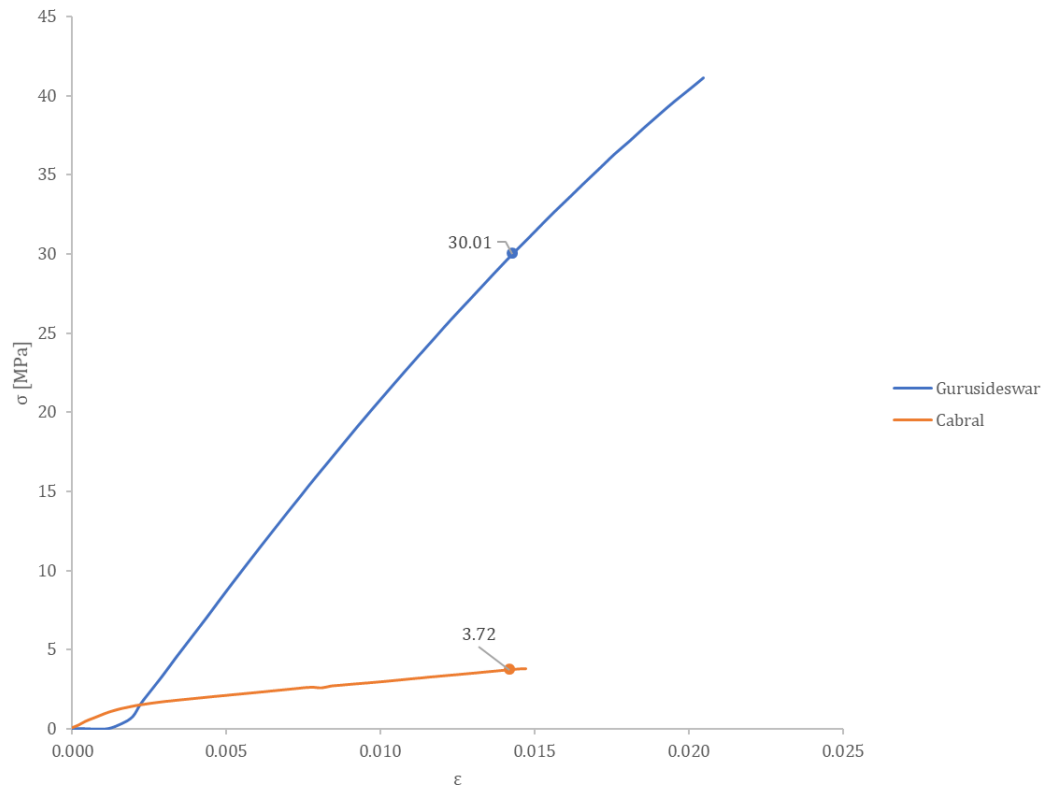


Figure 45. Epoxy curve used as input (orange), and epoxy curve tested experimentally (blue)

Both curves fail at around 1.5% and 2% deformation, but at different ultimate stress values on a different slope. Hence, the experimental result (Gurusideswar et al., 2017) used for comparison on Figure 44 is the best approximation given the available information.

Additionally, given the results on Figure 44, the *steep* slope of TEST1 does not follow the tendency of the other samples tested. As mentioned in the previous chapter, the diameter of glass fibers is around $20\ \mu\text{m}$, which is the same size as the mesh size on TEST1. Predictably, this caused the spike in the slope (Young's Modulus), and high comparable stress to the other curves for this sample; since most of the volume on the sample was occupied by the fiber, of a stiffer, and stronger material than the matrix. Comparably, all the other samples follow a similar tendency, with TEST2 and TEST3 most closely resembling the experimental results.

The visual stress distributions generated by ABAQUS on the last time iteration for all the samples will be attached on ATTACHMENT C at the end of this document.

CONCLUSIONS

1. A 3D virtual composite material microstructure finite element model was developed integrating two different isotropic materials to comparatively analyze the effects of mesh size, and material input.
2. Stress is uniform throughout the samples tested, except on sharp edges and proximity to the boundary regions, especially on the fiber material.
3. Sample TEST1 has the steepest slope, the highest stress level on failure, and the most divergence from all the samples tested, since its mesh size is essentially the same size as the feature diameter (fiber).
4. Difference in mesh size influences the mechanical response of the model tested. As mesh size increases, in most cases, the material response will involve higher stresses.
5. Material inputs, specifically the non-linear elastic response exhibited by the matrix has a high influence on the final behavior of the composite. Moreover, the stress-strain output generated by the composite is *restrained* by the non-linearity of the epoxy.
6. Regions closer to the highest stress concentrators as in Figure 42 and Figure 43, exhibit higher stresses independently of the material composition of the region.
7. Resistance to flow increases (higher stresses) based on the orientation to the applied load. A close orientation to the applied load, corresponds to a higher level of stress carried upon that feature.
8. Given the desired output results, Figure 44, the closest resemblance to one of the samples developed is TEST2. Meaning a further analysis on a mesh size of $40 \mu m^3$ is desirable.

REFERENCES

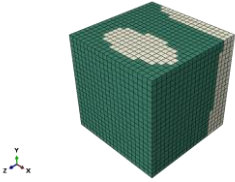
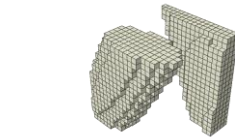
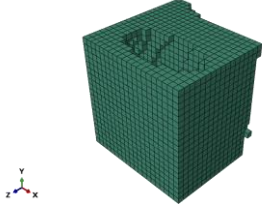
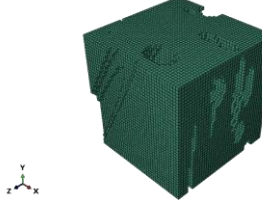
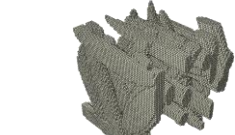
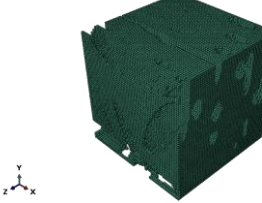
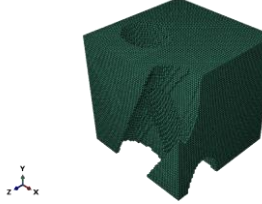
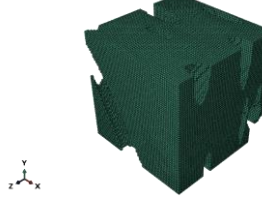
- Ashby, M. F. (2011). *Materials selection in mechanical design* (4th ed.). Kidlington, Oxford, UK: Elsevier.
- Barbero, E. J. (2011). *Introduction to Composite Materials Design 2nd ed - Ever J. Barbero* (CRC, 2011).
- Baus, J. (2016). Finite Element Modeling of Dual-Phase Polycrystalline Nickel-Base Alloys
Juan Fernando Baus Dobronsky Juan Fernando Baus Dobronsky.
- Cabral, K., & Boster, E. (2010). Mechanical Testing of Structural and Hybrid Epoxies, (May). Retrieved from http://instrumentation.tamu.edu/publications/Epoxy_Tests_Boster_Cabral_2010.pdf
- Cihan, M., Sobey, A. J., & Blake, J. I. R. (2019). Mechanical and dynamic performance of woven flax/E-glass hybrid composites. *Composites Science and Technology*, 172(January), 36–42. <https://doi.org/10.1016/j.compscitech.2018.12.030>
- Groeber, M. A. (n.d.). Generating Synthetic Microstructures w/ DREAM.3D: An Overview Tutorial. Retrieved from http://muri.materials.cmu.edu/wp-content/uploads/2015/06/DREAM3D_SyntheticMicrostructures.pdf
- Gurusideswar, S., Srinivasan, N., Velmurugan, R., & Gupta, N. K. (2017). Tensile Response of Epoxy and Glass/Epoxy Composites at Low and Medium Strain Rate Regimes. *Procedia Engineering*, 173, 686–693. <https://doi.org/10.1016/j.proeng.2016.12.148>
- Herakovich, C. T. (1997). *Mechanics of Fibrous Composites*. Wiley.
- Jackson, M. A. (2013). Digital Representation Environment for Analysis of Microstructure in Acknowledgements Mike Groeber (AFRL).
- Naghdinasab, M., Farrokhhabadi, A., & Madadi, H. (2018). A numerical method to evaluate the material properties degradation in composite RVEs due to fiber-matrix debonding and induced matrix cracking. *Finite Elements in Analysis and Design*, 146(April), 84–95. <https://doi.org/10.1016/j.finel.2018.04.008>
- Rohatgi, A. (2010). WebPlotDigitalizer. Retrieved from <https://automeris.io/WebPlotDigitizer/>
- Savvas, D., Stefanou, G., & Papadrakakis, M. (2016). Determination of RVE size for random composites with local volume fraction variation. *Computer Methods in Applied Mechanics and Engineering*, 305, 340–358. <https://doi.org/10.1016/j.cma.2016.03.002>
- Song, W., Krishnaswamy, V., & Pucha, R. V. (2016). Computational homogenization in RVE models with material periodic conditions for CNT polymer composites. *Composite Structures*, 137, 9–17. <https://doi.org/10.1016/j.compstruct.2015.11.013>
- Stasa, F. L. (2003). Applied Finite Element Analysis. *Computers & Mathematics with Applications*, 3(2), 154. [https://doi.org/10.1016/0898-1221\(77\)90080-3](https://doi.org/10.1016/0898-1221(77)90080-3)

- Tane, M., Okuda, H., & Tanaka, F. (2019). Acta Materialia Nanocomposite microstructures dominating anisotropic elastic modulus in carbon fibers, *166*, 75–84.
- Távora, L., Mantič, V., Graciani, E., & París, F. (2016). Modelling interfacial debonds in unidirectional fibre-reinforced composites under biaxial transverse loads. *Composite Structures*, *136*, 305–312. <https://doi.org/10.1016/j.compstruct.2015.09.034>
- Yang, X. (n.d.). Abaqus Tutorial.

ATTACHMENT A: INPUT DATA FOR THE *PLASTIC OPTION

FIBER			MATRIX		
No. point	ϵ	$\sigma, \text{N}/\mu\text{m}^2$	No. point	ϵ	$\sigma, \text{N}/\mu\text{m}^2$
1	0.00122	8.5629E-05	1	0.00033	0.000000032
2	0.00189	0.000171017	2	0.00076	0.000000053
3	0.00261	0.000241628	3	0.0012	0.000000032
4	0.00354	0.000300801	4	0.00227	0.000001672
5	0.00446	0.0003668	5	0.00291	0.000003265
6	0.00545	0.000457704	6	0.00338	0.000004495
7	0.00688	0.000582676	7	0.00386	0.000005718
8	0.00822	0.000692548	8	0.00436	0.000006983
9	0.00961	0.000812148	9	0.00478	0.000008088
10	0.01099	0.000929701	10	0.00518	0.00000913
11	0.01238	0.001048792	11	0.00565	0.000010306
12	0.01376	0.001163773	12	0.0061	0.000011431
13	0.01515	0.00128287	13	0.00655	0.00001257
14	0.01653	0.001400933	14	0.00699	0.00001365
15	0.01792	0.001515914	15	0.00742	0.000014684
16	0.0193	0.001634487	16	0.00784	0.000015709
17	0.02069	0.001753585	17	0.00833	0.000016868
18	0.02207	0.001868049	18	0.00879	0.000017959
19	0.02346	0.001988683	19	0.00924	0.000019027
20	0.02484	0.002109318	20	0.0097	0.000020069
21	0.02628	0.002228271	21	0.01066	0.000022246
22	0.02761	0.002342363	22	0.0111	0.000023196
23	0.029	0.002460426	23	0.01161	0.000024311
24	0.03051	0.002585763	24	0.01206	0.000025304
25	0.03189	0.00270486	25	0.01244	0.000026118
26	0.03328	0.002823434	26	0.01289	0.000027035
27	0.03467	0.002935333	27	0.01337	0.000028039
28	0.03605	0.003053396	28	0.01383	0.000029009
29	0.03744	0.003176085	29	0.01473	0.000030791
30	0.03882	0.003287984	30	0.0152	0.00003174
31	0.04021	0.003406557	31	0.01564	0.000032582
32	0.04159	0.003527192	32	0.01611	0.000033468
33	0.04298	0.003642691	33	0.01655	0.000034288
34	0.04436	0.003762298	34	0.01755	0.000036148
35	0.04575	0.003879844	35	0.01803	0.000036958
36	0.0471	0.00399035	36	0.0185	0.000037798
37	0.04852	0.004111861	37	0.019	0.000038647
38	0.0499	0.004230441	38	0.01951	0.000039501
39	0.05129	0.004349021	39	0.01999	0.000040253
40	0.05292	0.004484715	40	0.02043	0.000040949

ATTACHMENT B: TEST SAMPLE VISUALS

No.	Composite	Fiber	Matrix
1			
2			
3			
4	Same as above	Same as above	Same as above
9			
10			
11	Same as above	Same as above	Same as above

